«ФИЗИКА ЭЛЕМЕНТАРНЫХ ЧАСТИЦ И АТОМНОГО ЯДРА»
1998, ТОМ 29, ВЫП. 6

УДК 539.143, 539.142.2

INTERPLAY OF COLLECTIVE AND NONCOLLECTIVE MODES AT LOW EXCITATION ENERGY IN SPHERICAL NUCLEI

M.Grinberg, Ch.Stoyanov, N.Tsoneva

Institute for Nuclear Research and Nuclear Energy, BAS,
bul. Tzarigrad Road 72, 1784 Sofia, Bulgaria

«ФИЗИКА ЭЛЕМЕНТАРНЫХ ЧАСТИЦ И АТОМНОГО ЯДРА»
1998, ТОМ 29, ВЫП. 6

УДК 539.143, 539.142.2

INTERPLAY OF COLLECTIVE AND NONCOLLECTIVE MODES AT LOW EXCITATION ENERGY IN SPHERICAL NUCLEI

M.Grinberg, Ch.Stoyanov, N.Tsoneva

Institute for Nuclear Research and Nuclear Energy, BAS,
bul. Tzarigrad Road 72, 1784 Sofia, Bulgaria

The interplay of collective and noncollective excitations in spherical even-even nuclei is studied. This is done using a version of the Quasiparticle-Phonon Model (QPM) which accounts for up to three-phonon components in its excited-state wave functions and for the particle-particle channel of the residual interaction. Modes, ranging from single-particle ones to collective ones, with isoscalar and isovector nature and different multipolarity are included in the model basis. The structure of the low-lying, negative- and positive-parity states are calculated for semimagic and neighbouring nuclei. It is shown that the quasiparticle-phonon interaction is larger in the nuclei having two nucleons extra closed shell, and the three-phonon terms influence considerably the structure of the low-lying states. The low-lying $M1$ transitions linking 2^+ states are investigated. The presence and influence of a quadrupole low-lying isovector mode shared by several 2^+ states is displayed. The excited state structure of some N =84 nuclei, obtained in the QPM, is compared with the results of the Interacting Boson Model. The domains of similarity and discrepancy between both models are discussed. The properties of the low-lying 1^- states and corresponding $E1$ transitions are investigated for some N =82 nuclei. It is shown that these states can be interpreted as quadrupole-octupole two-phonon states and their characteristics result from the interplay of isovector and isoscalar modes. Some experimental evidences for the existence in ^{124}Te of negative parity three-phonon states, involving octupole excitations, are also discussed and comparison with QPM calculations is made.

Исследовано взаимодействие коллективных и неколлективных возбуждений в четно-четных сферических ядрах. Для этой цели использовалась квазичастично-фононная модель ядра. Волновая функция возбужденных состояний включала трехфононные компоненты. Учитывалось остаточное взаимодействие в канале частица-частица, а также изоскалярные и изовекторные компоненты частично-дырочного взаимодействия. В расчетах учитывалось большое одночастичное пространство.

Рассчитана структура низколежащих состояний положительной и отрицательной четности в полумагических и соседних с ними ядрах. Показано, что квазичастично-фононное взаимодействие сильнее в ядрах, имеющих на два нуклона больше, чем ядра с замкнутой оболочкой. Влияние трехфононных членов в этих ядрах велико. Исследованы $M1$-переходы между низколежащими 2^+-уровнями. Показано, что при низких энергиях возбуждения наличествует изовекторная квадрупольная сила, которая распределена по нескольким 2^+-уровням. Рассчитанная в рамках квазичастично-фононной модели структура низколежащих состояний в ядрах изотонов $N = 84$ сравнивается с той, что следует из модели взаимодействующих бозонов. Обсуждаются сходство и различия предсказаний моделей. Исследованы свойства низколежащих 1^--состояний и соответствующих $E1$-переходов в ядрах изотонов $N = 82$. Показано, что эти состояния с высокой степенью достоверности могут быть интерпретированы как двухфононные квадруполь-октупольные. Их свойства определяются тонкой игрой изоскалярных квадрупольной

и октупольной и изовекторной дипольной компонент остаточных сил. Обсуждаются экспериментальные доказательства существования трехфононных состояний отрицательной четности в ^{124}Te, которые затем сравниваются с предсказаниями квазичастично-фононной модели.

1. INTRODUCTION

As well known, the description of the structure and the properties of the excited states in medium and heavy nuclei is a complicated task. It is obvious *a priori* that no theory can account for all of the details of each individual nucleon motion, because of the large number of degrees of freedom. This fact has led to the formulation of various approaches, each convenient for a specific domain of problems. One important such domain is related to the existence in nuclei of collective modes [1], mainly evinced by large electromagnetic transitions and characteristic level spacing. Several models aimed at the problems related to collective states have been proposed and used. As far as collective vibrational states are concerned, there exist two lines of model development. The first of them starts from the expected microscopic structure of the excitations, namely keeps explicitly track of the underlying fermion structure. Such models, like the Quasiparticle Phonon Model (QPM) [2, 3] (also the Multiphonon model [4]), use phonons (RPA or TDA) as building blocks for constructing more complicated states. The second type of models, formulates the problems expressing the operators and wave functions in terms of superpositions of a few ideal bosons (e.g., boson expansion and mapping technics [5–7], the Interacting Boson Model (IBM) [8]). The former type of models typically uses a sophisticated wave function and relatively simple Hamiltonians. This is related to the fact that the phonons can incorporate excitations with a different degree of collectivity – from pure two-quasiparticle excitations to a superposition of many two-quasiparticle components. This rich basis, to be effectively used, requires the account for the Pauli principle, otherwise spurious solutions appear. It has been shown [3, 9, 18] that corrections due to the Pauli principle can be handled approximately in a relatively simple way. The interpretation of the results within models using ideal bosons makes necessary some mapping to the fermion space to be performed. Typically, the bosons in IBM are considered as counterparts of some two-fermion excitations. Both approaches have their virtues and drawbacks. The QPM, as representative of the so-called semimicroscopic models [2], has been used in the investigation of spherical and deformed nuclei at different energy domains. The large amount of results convincingly shows that this model gives valuable information on the properties of the collective modes, both at low and high energies, and on the fragmentation of these modes over the noncollective states in the spectrum. This makes it possible to describe subtle properties stemming from the interplay between collective and noncollective degrees of freedom. On the other hand, the ideal boson-based models, some of which use a considerable number

of parameters, describe in a smooth way the properties of groups of collective excited states (usually reflecting some dynamical symmetry of the Hamiltonian) throughout different nuclei. The latter gives the possibility of making systematics over a large number of nuclei. The drawback of these models, however, is the restricted basis, the large number of parameters and the lack of details in the description.

In spite of the usefulness of the IBM and of the QPM, the description they provide is only approximate. In the framework of IBM the noncollective degrees of freedom are neglected while the collective basis of QPM is very restricted. The new experimental information obtained by means of high-resolution multidetector systems points to a very complicated structure of the low-lying states. Even small admixtures are important to explain the observed values. Recent theoretical studies of energy-level statistics of low-lying excited states display a nearly Gaussian orthogonal ensemble distribution (see, e.g., [10]). The latter means that the nuclear dynamics is chaotic to a large extent, which suggests a complex interplay of many factors. An important place among them must be certainly reserved for the interplay between collective and noncollective modes, at least as far as the low-lying states are concerned.

In a number of papers [11–16], we have studied the low-lying excited states in medium and heavy even-even spherical nuclei in the framework of the QPM. Our main interest was concentrated on the increase of the collective basis of the model and the impact of the latter on the properties of the low-lying states. Until recently, the basis of the QPM was restricted to one- and two-phonon states. We have increased the number of phonons in the model wave function up to three [11, 14]. We want to present here the most important, in our view, results mainly concerning negative parity two- and three-phonon states involving quadrupole and octupole excitations.

Section 2 of this paper contains a concise but complete presentation of the QPM. In an Appendix a detailed presentation of the background of the model is presented, including some new results. The next five sections are devoted to different applications of the formalism in different groups of nuclei. Sections 3, 4, 5, and 6 are devoted to the description of dipole two-phonon states in nuclei with $N = 82$ and $N = 84$ and of isovector states in some N=84 nuclei. Section 7 presents the investigation of three-phonon negative parity states in ^{124}Te. In the conclusion, a summary of the main results is given and suggestions for further research, both theoretical and experimental, are formulated.

2. GENERAL DESCRIPTION OF THE MODEL

There are several textbooks [2,3] and review articles [17-19] where the main ideas of QPM are presented. In this section, we present in detail the extension

of the model, which consists in the incorporation of three-phonon components in the excited-state wave function.

Following Refs. 2,17 (see also the Appendix), we shall introduce some basic notations. Building blocks of the model basis are the quasiparticle RPA phonons defined as follows:

$$Q^{+}_{\lambda\mu i} = \frac{1}{2}\sum_{jj'}\left\{\psi^{\lambda i}_{jj'}A^{+}(jj';\lambda\mu) - (-1)^{\lambda-\mu}\phi^{\lambda i}_{jj'}A(jj';\lambda-\mu)\right\}, \qquad (1)$$

where the quantities j stand for all single-particle quantum numbers but the magnetic ones. The quantities $A^{+}(jj';\lambda\mu)$ and $A(jj';\lambda-\mu)$ (see eq. (27) in the Appendix) are two-quasiparticle creation and annihilation operators, respectively, coupled to angular momentum λ. Further, $\psi^{\lambda i}_{jj'}$ and $\phi^{\lambda i}_{jj'}$ are the forward and backward RPA amplitudes, respectively, defining a phonon with angular momentum λ and root number i. The obtained phonons are not boson operators and we use commutation relations which take care of their fermion structure [3], thus accounting for the violation of the Pauli principle. We will refer to the RPA phonon states using the notation $[\lambda^{\pi}_{i}]_{RPA}$. The phonons are of different degree of collectivity, from collective ones (e.g., $[2^{+}_{1}]_{RPA}$) to pure two-quasiparticle configurations.

The following commutation relations can be obtained if the fermion structure of the phonon operators is taken into account:

$$\begin{aligned}
&\left[Q_{\lambda\mu i}, Q^{+}_{\lambda'\mu' i'}\right] = \delta_{\lambda\mu,\lambda'\mu'}\frac{1}{2}\sum_{jj'}\left(\psi^{\lambda i}_{jj'}\psi^{\lambda i'}_{jj'} - \phi^{\lambda i}_{jj'}\phi^{\lambda i'}_{jj'}\right) - \\
&\sum_{jj'j_2}\Big\{\psi^{\lambda i}_{j'j_2}\psi^{\lambda' i'}_{jj_2}\langle j'm'\ j_2m_2|\lambda\mu\rangle\langle jm\ j_2m_2|\lambda'\mu'\rangle \\
&-(-1)^{\lambda+\mu+\lambda'+\mu'}\phi^{\lambda i}_{jj_2}\phi^{\lambda' i'}_{j'j_2}\langle jm\ j_2m_2|\lambda-\mu\rangle\langle j'm'\ j_2m_2|\lambda'-\mu'\rangle\Big\}\,\alpha^{+}_{jm}\alpha_{j'm'},
\end{aligned} \qquad (2)$$

where $Q^{+}_{\lambda\mu i}$ is defined in eq. (1). The quantities $\langle j'm'\ j_2m_2|\lambda\mu\rangle$ are the Clebsch-Gordan coefficients. The operators α^{+}_{jm} and α_{jm} are the creation and annihilation quasiparticle operators, introduced by eq. (23). The double commutator of the phonon operators, taken in the so-called diagonal approximation (i.e., preserving the orthogonality of the two-phonon states), reads [3]:

$$\begin{aligned}
&\left[\left[Q_{\lambda_1\mu_1 i_1}, Q^{+}_{\lambda_1\mu_1 i_1}\right], Q^{+}_{\lambda_2\mu_2 i_2}\right] = \\
&\frac{1}{2}\sum_{\substack{\lambda'_2\mu'_2 i'_2\\ Ikl}}\left(\delta_{\lambda_1\mu_1,\lambda'_1\mu'_1}\delta_{\lambda_2\mu_2,\lambda'_2\mu'_2} + (-)^{\lambda_1+\lambda_2-I}\delta_{\lambda_1\mu_1,\lambda'_2\mu'_2}\delta_{\lambda_2\mu_2,\lambda'_1\mu'_1}\right)\times \\
&\langle\lambda_1\mu_1\ \lambda_2\mu_2|Ik\rangle\langle\lambda'_1\mu'_1\ \lambda'_2\mu'_2|Ik\rangle K^{I}(\lambda_1 i_1\,\lambda_2 i_2)\ Q^{+}_{\lambda'_2\mu'_2 i'_2},
\end{aligned} \qquad (3)$$

where

$$K^I(\lambda_1 i_1\, \lambda_2 i_2) = \hat{\lambda}_1 \hat{\lambda}_2 (2 - \delta_{\lambda_1 \lambda_2} \delta_{i_1 i_2}) \times \sum_{\substack{j_1 j_2 j_3 j_4 \\ m_1 m_2 m_3 m_4}} \left(\psi^{\lambda_1 i_1}_{j_1 j_2} \psi^{\lambda_2 i_2}_{j_2 j_4} \psi^{\lambda_1 i_1}_{j_1 j_3} \psi^{\lambda_2 i_2}_{j_2 j_4} - \phi^{\lambda_1 i_1}_{j_1 j_2} \phi^{\lambda_2 i_2}_{j_2 j_4} \phi^{\lambda_1 i_1}_{j_1 j_3} \phi^{\lambda_2 i_2}_{j_2 j_4} \right) \left\{ \begin{array}{ccc} j_1 & j_2 & \lambda_1 \\ j_3 & j_4 & \lambda_2 \\ \lambda_1 & \lambda_2 & I \end{array} \right\} \tag{4}$$

the quantity in curly brackets is a $9j$ symbol [20] and here and further $\hat{\lambda} = \sqrt{2\lambda + 1}$.

The model Hamiltonian in terms of phonons reads:

$$\begin{aligned} H &= \sum_{\lambda \mu i} \omega_{\lambda i} Q^+_{\lambda \mu i} Q_{\lambda \mu i} + \frac{1}{2} \sum_{\substack{\lambda_1 \lambda_2 \lambda_3 \\ i_1 i_2 i_3 \\ \mu_1 \mu_2 \mu_3}} \langle \lambda_1 \mu_1\, \lambda_2 \mu_2 | \lambda_3 - \mu_3 \rangle \times \\ & U^{\lambda_1 i_1}_{\lambda_2 i_2}(\lambda_3 i_3) [Q^+_{\lambda_1 \mu_1 i_1} Q^+_{\lambda_2 \mu_2 i_2} Q_{\lambda_3 - \mu_3 i_3} + h.c.]. \end{aligned} \tag{5}$$

The quantities $\omega_{\lambda i}$ denote the energies of the RPA phonons. The matrix elements $U^{\lambda_1 i_1}_{\lambda_2 i_2}(\lambda_3 i_3)$ are defined in eq. (45) in the Appendix.

The Hamiltonian (5) is diagonalized in a basis of wave functions constructed as a superposition of one-, two- and three-phonon components [14]:

$$\begin{aligned} \Psi_\nu(JM) &= \Big\{ \sum_i R_i(J\nu) Q^+_{JMi} + \sum_{\substack{\lambda_1 i_1 \\ \lambda_2 i_2}} P^{\lambda_1 i_1}_{\lambda_2 i_2}(J\nu) \left[Q^+_{\lambda_1 i_1} Q^+_{\lambda_2 i_2} \right]_{JM} \\ & + \sum_{\substack{\lambda_1 i_1 \\ \lambda_2 i_2 \\ \lambda_3 i_3 I}} T^{\lambda_1 i_1 \lambda_2 i_2}_{I\ \ \lambda_3 i_3}(J\nu) \left[\left[Q^+_{\lambda_1 i_1} Q^+_{\lambda_2 i_2} \right]_I Q^+_{\lambda_3 i_3} \right]_{JM} \Big\} \Psi_0, \end{aligned} \tag{6}$$

where $[\ldots]_{JM}$ stands for angular momentum coupling, Ψ_0 represents the phonon vacuum state and the coefficients R, P, and T are unknown amplitudes. The index ν specifies the particular excited state.

The normalization condition reads:

$$\begin{aligned} & < \Psi_\nu(JM) \mid \Psi_\nu(JM) > = \\ & = \sum_i \left[R_i(J\nu) \right]^2 + 2 \sum_{\lambda_1 i_1 \lambda_2 i_2} \left[P^{\lambda_1 i_1}_{\lambda_2 i_2}(J\nu) \right]^2 \overline{K^I}(\lambda_1 i_1\, \lambda_2 i_2) + \\ & \quad + 6 \sum_{\substack{\lambda_1 i_1 \\ \lambda_2 i_2 \\ \lambda_3 i_3 I}} \left[T^{\lambda_1 i_1 \lambda_2 i_2}_{I\ \ \lambda_3 i_3}(J\nu) \right]^2 C^J_I(\lambda_1 i_1, \lambda_2 i_2, \lambda_3 i_3) = 1, \end{aligned} \tag{7}$$

where

$$\overline{K^I}(\lambda_1 i_1\, \lambda_2 i_2) = 1 + \frac{1}{2} K^I(\lambda_1 i_1\, \lambda_2 i_2)$$

and

$$C_I^J(\lambda_1 i_1,\, \lambda_2 i_2,\, \lambda_3 i_3) = 1 + \frac{3}{2} K^I(\lambda_1 i_1\, \lambda_2 i_2)$$
$$+\frac{1}{2} K^I(\lambda_1 i_1\, \lambda_2 i_2) \sum_{I'} \left[\overline{U}(\lambda_1 \lambda_2 J \lambda_3; I,\, I')\right]^2 K^{I'}(\lambda_2 i_2\, \lambda_3 i_3).$$

The quantities K account for the Pauli principle and are defined through eq. (4). The quantities $\overline{U}$ stand for the Jahn coefficients [20] (this somewhat unusual notation is used to distinguish these quantities from the matrix elements U defined by eq. (45)). After applying a variational procedure [3], a system of equations can be written in the following form:

$$\left|\begin{array}{l} (\omega_{Ji} - \eta_{J\nu}) R_i(J\nu) - \displaystyle\sum_{\lambda_1 i_1 \lambda_2 i_2} P^{\lambda_1 i_1}_{\lambda_2 i_2}(J\nu) U^{\lambda_1 i_1}_{\lambda_2 i_2}(Ji) \overline{K^J}(\lambda_1 i_1\, \lambda_2 i_2) = 0 \\ \\ \left[\omega_{\lambda_1 i_1} + \omega_{\lambda_2 i_2} - \eta_{J\nu}\right] P^{\lambda_1 i_1}_{\lambda_2 i_2}(J\nu) - \dfrac{1}{2} \displaystyle\sum_{i'} U^{\lambda_1 i_1}_{\lambda_2 i_2}(Ji') R_{i'}(J\nu) \\ \qquad -3 \displaystyle\sum_{\lambda_1' i_1' \lambda_2' i_2'} T^{\lambda_1' i_1' \lambda_2' i_2'}_{\lambda_1 \lambda_2 i_2}(J\nu) U^{\lambda_1' i_1'}_{\lambda_2' i_2'}(\lambda_1 i_1) C^J_{\lambda_1}(\lambda_1' i_1' \lambda_2' i_2' \lambda_2 i_2) = 0 \\ \\ \left[\omega_{\lambda_1' i_1'} + \omega_{\lambda_2' i_2'} + \omega_{\lambda_3' i_3'} - \eta_{J\nu}\right] T^{\lambda_1' i_1' \lambda_2' i_2'}_{I \lambda_3' i_3'}(J\nu) - \\ \qquad \displaystyle\sum_{i''} P^{I i''}_{\lambda_3' i_3'}(J\nu) U^{\lambda_1' i_1'}_{\lambda_2' i_2'}(Ji'') \overline{K^J}(Ii''\, \lambda' i') = 0, \end{array}\right. \tag{8}$$

where $\eta_{J\nu}$ is the energy of the excited state υ with angular momentum J.

The coefficients R and T can be expressed as functions of the coefficients P and the system of equations can be rewritten as a system of equations only for the coefficients P. The corresponding expressions are:

$$R_{i'}(J\nu) = \frac{\displaystyle\sum_{\lambda_1 i_1 \lambda_2 i_2} P^{\lambda_1 i_1}_{\lambda_2 i_2}(J\nu) U^{\lambda_1 i_1}_{\lambda_2 i_2}(Ji) \overline{K^J}(\lambda_1 i_1\, \lambda_2 i_2)}{\omega_{Ji} - \eta_{J\nu}},$$

$$T^{\lambda_1' i_1' \lambda_2' i_2'}_{I \lambda_3' i_3'}(J\nu) = \frac{\displaystyle\sum_{i''} P^{I i''}_{\lambda_3' i_3'}(J\nu) U^{\lambda_1' i_1'}_{\lambda_2' i_2'}(Ii'') \overline{K^J}(Ii''\, \lambda_3' i_3')}{\omega_{\lambda_1' i_1'} + \omega_{\lambda_2' i_2'} + \omega_{\lambda_3' i_3'} - \eta_{J\nu}}.$$

After substitution in the second equation of the system of equations (8), we obtain:

$$\left[\omega_{\lambda_1 i_1} + \omega_{\lambda_2 i_2} - \eta_{J\nu}\right] P^{\lambda_1 i_1}_{\lambda_2 i_2}(J\nu) -$$
$$-\frac{1}{2} \sum_{\lambda_1' i_1' \lambda_2' i_2'} \sum_{i'} U^{\lambda_1 i_1}_{\lambda_2 i_2}(Ji') \frac{P^{\lambda_1' i_1'}_{\lambda_2' i_2'}(J\nu) U^{\lambda_1' i_1'}_{\lambda_2' i_2'}(Ji) \overline{K^J}(\lambda_1' i_1'\, \lambda_2' i_2')}{\omega_{Ji} - \eta_{J\nu}} -$$

$$-3\sum_{\lambda_1' i_1' \lambda_2' i_2'}\sum_{i''} U^{\lambda_1' i_1'}_{\lambda_2' i_2'}(\lambda_1 i_1) C^J_{\lambda_1}(\lambda_1' i_1', \lambda_2' i_2', \lambda_2 i_2)\times$$

$$\times\frac{P^{\lambda_1' i''}_{\lambda_2' i_2'}(J\nu) U^{\lambda_1' i_1'}_{\lambda_2' i_2'}(\lambda_1 i'')\overline{K^J}(\lambda_1 i''\,\lambda_2' i_2')}{\omega_{\lambda_1' i_1'} + \omega_{\lambda_2' i_2'} + \omega_{\lambda_3 i_3} - \eta_{J\nu}} = 0.$$

In the general derivation of the above equations [3] (without a diagonal approximation for the quantities K), for the two-phonon case, energy shifts of the two-phonon poles appear. They are due to the inclusion of Hamiltonian terms which do not contribute in RPA, but contribute when the exact commutation relations between phonons are taken into account in QPM. In fact, the energy shifts are proportional to only nondiagonal quantities K. In the derivation here, we use the diagonal approximation from the very beginning and that is why such shifts don't appear in eqs. (8). Moreover, the shifts of the two-phonon poles are estimated to be small in spherical nuclei [3].

The electric transition operator in terms of phonons reads [2]:

$$\begin{aligned} M(E\lambda) \;=\; & \sum_{\mu i} X_i(E\lambda)\,(Q^+_{\lambda\mu i} + (-1)^{\lambda-\mu} Q_{\lambda-\mu i}) \\ & + \sum_{\substack{\lambda_1\mu_1 i_1 \\ \lambda_2\mu_2 i_2\mu}} \langle \lambda_1\mu_1\ \lambda\mu|\lambda_2\mu_2\rangle \Big[F^{\lambda_1 i_1}_{\lambda_2 i_2}(E\lambda)\, Q^+_{\lambda_2\mu_2 i_2} Q_{\lambda_1\mu_1 i_1} \\ & + \overline{F}^{\lambda_1 i_1}_{\lambda_2 i_2}(E\lambda)\,\Big(Q^+_{\lambda_2\mu_2 i_2} Q^+_{\lambda_1\mu_1 i_1} + h.c.\Big)\Big], \end{aligned} \tag{9}$$

where

$$X_i(\lambda,\tau) = \sum_{jj'} f^{\lambda tr}_{jj'} u^{(+)}_{jj'} (\psi^{\lambda i}_{jj'} + \varphi^{\lambda i}_{jj'}),$$

$$F^{\lambda_1 i_1}_{\lambda_2 i_2}(\lambda,\tau) = \hat\lambda_1\hat\lambda_2 \sum_{jj'j''} {}^{\tau} f^{\lambda tr}_{jj'} v^{(-)}_{jj'} \left\{ \begin{array}{ccc} \lambda_1 & \lambda_2 & \lambda \\ j & j' & j'' \end{array} \right\} \Big(\psi^{\lambda_1 i_1}_{j'j''}\phi^{\lambda_2 i_2}_{j''j} + \phi^{\lambda_1 i_1}_{j'j''}\psi^{\lambda_2 i_2}_{j''j}\Big),$$

$$\bar F^{\lambda_1 i_1}_{\lambda_2 i_2}(\lambda,\tau) = \hat\lambda_1\hat\lambda_2 \sum_{jj'j''} {}^{\tau} f^{\lambda tr}_{jj'} v^{(-)}_{jj'} \left\{ \begin{array}{ccc} \lambda_1 & \lambda_2 & \lambda \\ j & j' & j'' \end{array} \right\} \Big(\psi^{\lambda_1 i_1}_{j'j''}\psi^{\lambda_2 i_2}_{j''j} + \phi^{\lambda_1 i_1}_{j'j''}\phi^{\lambda_2 i_2}_{j''j}\Big).$$

The quantities $f^{\lambda tr}_{jj'}$ are the single-particle transition matrix elements, the quantities in the curly brackets are the $6j$ symbols [20].

Using the operator (9) and the excited state wave function (6), we obtain for the reduced transition probabilities the following expressions:

$$B(E\lambda; 0^+_{\rm g.s.} \to J\nu) = \frac{1}{\hat\lambda^2}\left|\sum_\tau e^{(\lambda)}_{\rm eff}(\tau)\left[\sum_i X_i(\lambda,\tau) R_i(J\nu) - \sum_{\lambda_1 i_1 \lambda_2 i_2} F^{\lambda_1 i_1}_{\lambda_2 i_2}(\lambda,\tau) P^{\lambda_1 i_1}_{\lambda_2 i_2}(J\nu)\right]\right|^2, \tag{10}$$

$$B(E\lambda; I\rho \to J\nu) = \left[\frac{\hat{J}}{\hat{I}}\right]^2 \left| \sum_\tau e^{(\lambda)}_{\rm eff}(\tau) \left[-\hat{J}^{-1} \sum_i \bar{F}^{Ii'}_{Ji}(\lambda,\tau) R_i(J\nu) R_{i'}(I\rho) - \right.\right.$$
$$\hat{I} \sum_{\lambda_1 i_1 \lambda_2 i_2 \lambda' i'} \bar{F}^{\lambda_1 i_1}_{\lambda_2 i_2}(\lambda,\tau) P^{\lambda_1 i_1}_{\lambda' i'}(J\nu) P^{\lambda' i'}_{\lambda_2 i_2}(I\rho) \left\{ \begin{array}{ccc} J & I & \lambda \\ \lambda_2 & \lambda_1 & \lambda' \end{array} \right\} +$$
$$+\hat{\lambda}^{-1} \sum_{ii'} X_i(\lambda,\tau) \left[R_{i'}(I\rho) P^{Ii'}_{\lambda i}(J\nu) + \frac{\hat{I}}{\hat{J}} P^{Ii'}_{\lambda i}(I\rho) R_{i'}(J\nu) \right] -$$
$$-\hat{\lambda}^{-1} \sum_{\lambda_1 i_1 \lambda_2 i_2 i'} F^{\lambda_1 i_1}_{\lambda_2 i_2}(\lambda,\tau) \left[\frac{\hat{I}}{\hat{J}} R_{i'}(I\rho) T^{\lambda_1 i_1 \lambda_2 i_2}_{\lambda \quad Ii'}(J\nu) + T^{\lambda_1 i_1 \lambda_2 i_2}_{\lambda J i'}(I\rho) R_{i'}(J\nu) \right] +$$
$$+ \; 3\hat{\lambda}^{-1} \sum_i X_i(\lambda,\tau) \sum_{\lambda_1 i_1 \lambda_2 i_2} \times$$
$$\left. \left. \times \left[P^{\lambda_1 i_1}_{\lambda_2 i_2}(I\rho) T^{\lambda_1 i_1 \lambda_2 i_2}_{I \quad \lambda i'}(J\nu) + \frac{\hat{I}}{\hat{J}} T^{\lambda_1 i_1 \lambda_2 i_2}_{J \lambda i'}(I\rho) P^{\lambda_1 i_1}_{\lambda_2 i_2}(J\nu) \right] \right] \right|^2 . \tag{11}$$

3. THE STRUCTURE OF LOW-LYING EXCITED STATES IN THE SEMIMAGIC $N = 82$ AND THE NEIGHBOURING $N = 84$ EVEN-EVEN NUCLEI

The low-energy spectrum of the atomic nuclei reveals interesting features of the interplay between collective and noncollective excitations. The observed effects are related to the initial stage of the dissipation of the collective properties in atomic nuclei. Usually, the phenomenon is associated with the excitation energies in the domain of giant resonances, where the interaction of the collective mode with surface vibrations leads to its damping and it is seen as a large spreading width of the collective state [19, 21]. At low excitation energies the strength of the collective mode usually is shared between several excited states, but in some cases the strength is distributed within a few hundred keV energy range. This effect is very well established in the magic, semimagic and their neighbouring nuclei. A schematic picture presented in Fig.1 explains qualitatively the reason for that. The two nuclei ^{144}Sm (semimagic N =82) and ^{144}Nd (having two neutrons extra closed shell) are discussed. The energies of the two-quasiparticle states with $J^\pi = 2^+$ are plotted. It is seen for both nuclei that the energies of several 2^+ two-quasiparticle states are between 2.5 and 4.0 MeV. On the other hand, the properties of the first 2^+ state in both nuclei are very different. The first 2^+ state in ^{144}Nd is a collective state ($B(E2; 2^+_1 \to$ g.s.)=16 W.u.) and its energy is relatively far from the first group of two-quasiparticle states. The ^{144}Nd is a vibrational nucleus and the two-phonon quadrupole states are expected at excitation energy

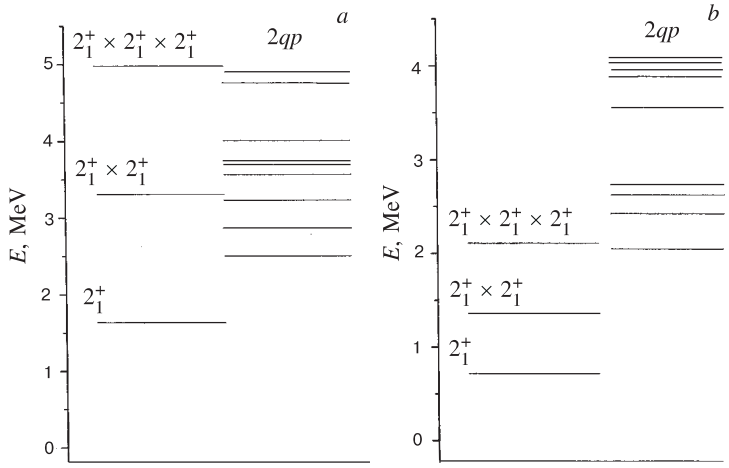

Fig. 1. Non-perturbed energy (i.e. the sum of the energies of the constituent RPA phonons) of one-, two- and three-phonon states with $J^\pi = 2^+$ and energies of the two-quasiparticle states in (a) ^{144}Sm and (b) ^{144}Nd

equal to twice the energy of the first 2^+ state. The energy of the expected triplet is plotted in Fig. 1. It is seen that the triplet and the two-quasiparticle states are at least 1 MeV apart. The energy of the 2_1^+ state in ^{144}Sm displays a different picture. Its energy is 1.628 MeV and it is a collective state (seen from the large $B(E2)$=13 W.u., which is however smaller than the corresponding value for ^{144}Nd), but the energy of the expected two-phonon quadrupole-quadrupole multiplet is around 3.2 MeV – just in the middle of the two-quasiparticle group. The comparison of these two nuclei leads to the conclusion that the strength of the two-phonon states in ^{144}Sm could be fragmented over several excited states, while for ^{144}Nd one could expect more concentrated two-phonon components. This effect, for semimagic nuclei, has been investigated in Refs. 22,23. The latter is seen from Fig. 2, which presents the distribution of the $[2_1^+ \otimes 2_1^+]_{2^+}$ component over 2^+ states in ^{144}Nd and ^{144}Sm. The calculations were performed using the wave function (6). The histograms are in agreement with the above considerations. The two-phonon $[2_1^+ \otimes 2_1^+]_{2^+}$ component is shared between two states in ^{144}Nd and the larger portion is concentrated in the 1.7 MeV excited state. The two-phonon component in ^{144}Sm is distributed over several states within 1 MeV energy range. This example demonstrates that the properties of the low-lying states around closed shells are very sensitive to the details of the fragmentation of the two-phonon components of the wave function (6). The last statement raises the question about the dependence of the presented results on the size of the collective basis. In QPM, the influence of the three-phonon term on the

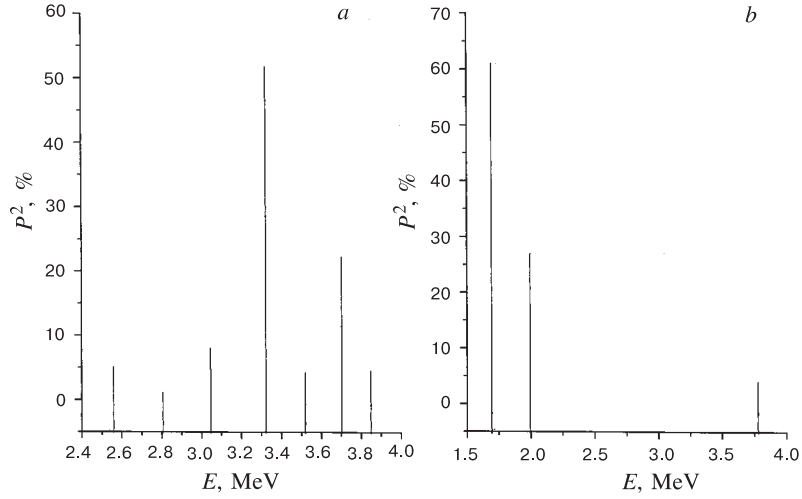

Fig. 2. Distribution of the two-phonon $[2_1^+ \times 2_1^+]_{2^+}$ component in (a) ^{144}Sm and (b) ^{144}Nd

two-phonon one is crucial, as it can be seen from eqs. (5) and (45). The model interaction mixes states differing by one phonon. This is the reason, why four- and more complicated multiphonon states would change the distribution of the two-phonon component much less than the three-phonon states. Some examples are given in Table 1 *. In general, the energies of the excited states are not very sensitive to the basis. For example, the energy of 2_2^+ state in ^{144}Nd is changed from 1.772 MeV to 1.730 MeV when the three-phonon components are taken into account (see Table 7).

Quantities bearing much interesting information are the $B(E2)$ values involving the states with a large two-phonon $[2_1^+ \otimes 2_1^+]_{2^+}$ component. As shown in Fig. 2, such states are the 2_2^+ and 2_3^+ states in ^{144}Nd and the 2_5^+ state in ^{144}Sm (in Fig. 2, the notation 2_{22}^+ is used for the 2_5^+ state, to stress the dominance of the $[2_1^+ \otimes 2_1^+]_{2^+}$ component in the structure of this state). It is seen that the influence of the three-phonon terms is more important for ^{144}Nd than for ^{144}Sm. The reason for this effect is the different collectivity of the quadrupole phonon in both nuclei. The larger collectivity of the 2_1^+ state in ^{144}Nd leads to larger quasiparticle-phonon interaction matrix element (45) and consequently to a larger coupling of the two- and three-phonon quadrupole components, which increase the contribution of the $[2_1^+ \otimes 2_1^+]_{2^+}$ component in the wave function (see Table 7).

*Tables 4 and 7 contain the energies and the structure of the excited-state wave function for two cases – with and without the three-phonon components in the basis.

Table 1. Relative influence of the three-phonon component of the wave function (6) on the $B(E2)$ value in QPM

	$B(E2)$	Exp. $[e^2b^2]$	QPM with 3ph. $[e^2b^2]$	QPM without 3ph. $[e^2b^2]$	3 ph. effect [%]
^{144}Nd	$2_2^+ \to$ g.s.	0.001(1)$^{(a)}$	0.0020	0.0036	44
	$2_3^+ \to$ g.s.	0.0045$^{(b)}$	0.0073	0.0054	35
	$2_2^+ \to 2_1^+$	0.095(21)$^{(a)}$	0.1200	0.0840	43
	$2_3^+ \to 2_1^+$	0.020(10)$^{(a)}$	0.0400	0.0560	29
^{144}Sm	$2_5^+ \to 2_1^+$	-	0.0821	0.0816	0.6
	$2_5^+ \to$ g.s.	-	0.0006	0.0006	0

^{a}Taken from Refs. 31,33.
^{b}Taken from Ref. 26.

For example, depending on the basis, the contribution of the $[2_1^+ \otimes 2_1^+]_{2^+}$ component in the 2_2^+ states is changed from 48% (in the case when the three-phonon components are not taken into account) to 61% (in the case when the three-phonon components are taken into account). A similar redistribution is found for the 2_3^+ state in ^{144}Nd, while the structure of the two-phonon 2_5^+ state in ^{144}Sm is unchanged by the interaction with three-phonon components (see Table 4). Table 1 convincingly shows that the influence of the three-phonon components is more important for the N =84 nuclei than for the semimagic N =82 nuclei.

Table 2. Parameters of the Woods-Saxon potential (A=141, Z=59)

	r $[fm]$	V_0 [MeV]	κ $[fm^2]$	α $[fm^{-1}]$
N	1.27	45.95	0.413	1.613
Z	1.31	53.435	0.349	1.538

The parameters that have been used in the calculations are the following. The parameters of the Woods-Saxon potential are taken from Refs. 24,25 (see Table 2) and the relevant part of the obtained single-particle spectrum can be found in Fig.3. The pairing coupling constants are chosen according to Ref. 2. For the mass region A≈144, the values of the pairing constants $G_{\rm n}$ and $G_{\rm p}$ are 0.116 MeV and 0.119 MeV, respectively. The radial dependence of the separable multipole interaction is taken in the form $f(r) \sim {\rm d}V(r)/{\rm d}r$, where $V(r)$ represents the

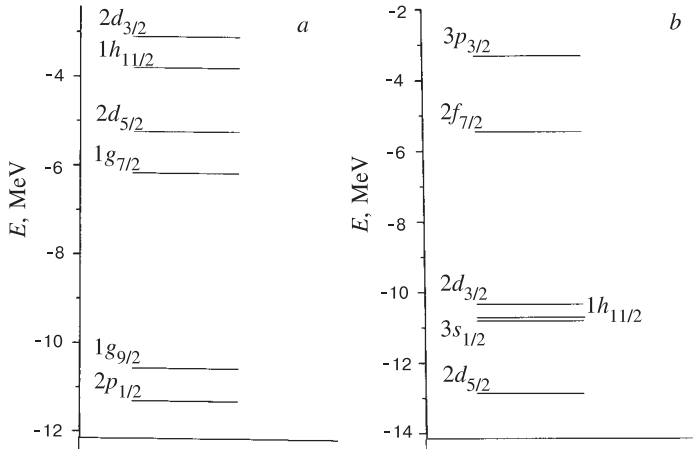

Fig. 3. Energies of the (a) proton and (b) neutron single-particle states for A=141 (only the states around the Fermi level are plotted)

central part of the Woods-Saxon potential. The separable interaction strength is considered as a phenomenological parameter fixed so as to reproduce the experimental energy of the corresponding lowest collective states for the states with $J^\pi = 2^+$ and 3^-. For the rest of the multipolarities, the first RPA root energy is usually fixed to be close to the first two-quasiparticle state energy [17]. In the cases, when the reliable experimental information shows that a particular lowest state has a collective component, the parameters are fixed in the same way as for the quadrupole and octupole collective states. In the present investigation, this is the case of the 4_1^+ state in ^{144}Nd [26]. The particle-particle channel is included only for $J^\pi = 2^+$ and 3^- . The strength of the interaction in this channel between protons and between neutrons has been taken to be $G_p^{(2)} = G_n^{(2)} = 0.8$—$0.85\ \kappa_0^{(2)}$ and $G_p^{(3)} = G_n^{(3)} = 0.6$—$0.7\ \kappa_0^{(3)}$ for the multipolarities 2^+ and 3^-, respectively. Here, $\kappa_0^{(2)}$ ($\kappa_0^{(3)}$) is the isoscalar quadrupole (octupole) parameter for the particle-hole separable residual interaction. In the present calculation, phonons with $\lambda^\pi = 1^-$, 2^+, 3^-, 4^+, 5^- and 6^+ and several roots for each multipolarity are included. The isovector constant for the 1^- states is chosen in a way to reproduce correctly the energy of the isovector dipole resonance.

The structure of the low-lying states is calculated for several nuclei with $N = 84$ (^{140}Ba, ^{142}Ce, ^{144}Nd, and ^{146}Sm) and $N = 82$ (^{138}Ba, ^{140}Ce, ^{142}Nd, and ^{144}Sm). In general, the parameters used for the considered nuclei coincide within 5%.

For the RPA positive parity states with low energy and $J \leq 6$ in the N=82 isotones, the main contribution comes from the single-particle proton configura-

tions $1g_{7/2}$ and $2d_{5/2}$. The latter correspond to the filled subshells in ^{138}Ba and ^{140}Ce and in ^{142}Nd and ^{144}Sm, respectively. The $[2_1^+]_{RPA}$ state is a collective one, containing $\pi[1g_{7/2}]^2$ ($\sim$ 35 %) and $\pi\left[2d_{5/2}\right]^2$ ($\sim$ 22 %) as major components for ^{140}Ce and ^{138}Ba. The main component for ^{144}Sm (see Table 3) and ^{142}Nd are $\pi\left[2d_{5/2}\right]^2$ ($\sim$ 34 %) and $\pi\left[1h_{11/2}\right]^2$ ($\sim$ 22 %). The other collective RPA state is the $[3_1^-]_{\rm RPA}$ state. The $[3_1^-]_{\rm RPA}$ state obtained in our calculations contains 74 % of the $\pi\left[2d_{5/2}1h_{11/2}\right]$ configuration and smaller admixtures of the $\nu\left[3s_{1/2}2f_{7/2}\right]$ and $\pi[1g_{7/2}1h_{11/2}]$ configurations, which is consistent with the estimates given in Refs. 27,28. A detailed analysis of the structure of the RPA states within QPM for ^{142}Nd can be found also in Ref. 28.

Table 3. Structure of some RPA phonons (only components exhausting more than 5% are quoted) and values of $B(E\lambda)\uparrow$ for ^{144}Sm

λ_i^π	$\omega_{\lambda_i^\pi}$[MeV]	Structure	$B(E2)\uparrow$ [W.u.]
2_1^+	1.700	$4\%\nu[1h_{11/2}2f_{7/2}] + 34\%\pi[2d_{5/2}]^2$	71.6
		$+22\%\pi[1h_{11/2}]^2 + 8\%\pi[2d_{5/2}3s_{1/2}]$	
		$+7\%\pi[1g_{7/2}2d_{3/2}] + 7\%\pi[1g_{7/2}]^2$	
2_2^+	2.678	$62\%\pi[2d_{5/2}]^2 + 13\%\pi[1h_{11/2}]^2$	5.5
		$+10\%\pi[1g_{7/2}2d_{5/2}]$	
2_3^+	2.876	$87\%\pi[1g_{7/2}2d_{5/2}] + 6\%\pi[1h_{11/2}]^2$	1.5
2_4^+	3.146	$87\%\pi[1g_{7/2}]_p^2 + 10\%\pi[1h_{11/2}]^2$	0.02
3_1^-	1.900	$74\%\pi[2d_{5/2}1h_{11/2}]$	268.8
4_1^+	2.425	$94\%\pi[2d_{5/2}]^2$	53.2

The structure of some excited states in ^{144}Sm is given in Table 4. The first excited 2^+ and 3^- states described by (6) are composed mainly of the corresponding collective RPA phonons ($>$ 90 %, see Table 4). The comparison between the calculated and experimental values for the $B(E2)$ and $B(E3)$ rates from these states to the ground state can be found in Table 10.

Due to the magic number of neutrons, the low-lying excited states of N =82 nuclei are expected to be mainly of noncollective character. Nevertheless, the reduced $E2$ and $E3$ transition probabilities from the first 2^+ and 3^- states, respectively, are larger than 10 W.u., which indicates their collective nature [29, 30]. It should be pointed out that the general trend of decrease of the 3_1^- state energy [27, 28], going from ^{138}Ba to ^{144}Sm, is reproduced in our calculations with only slight changes of the parameters. The better agreement

of our results with experiment, concerning the 3_1^- states, in comparison with the agreement of the results from Ref. 27, is due to the large basis of single-particle components taken into account.

Table 4. Energies and structure of the first 2^+, 3^- and 4^+ states in ^{144}Sm. Only the main components are presented

State	Exp.	QPM with 3 ph.		QPM without 3 ph.	
	E [MeV]	E [MeV]	Structure [%]	E [MeV]	Structure [%]
2_1^+	1.660	1.628	$96.9\%[2_1^+]_{\rm RPA}+$ $+2.7\%[3_1^-\otimes 3_1^-]$	1.628	$96.9\%[2_1^+]_{\rm RPA}$ $+2.7\%[3_1^-\otimes 3_1^-]$
2_2^+	2.423	2.560	$78\%[2_2^+]_{\rm RPA}$ $+5.8\%[2_1^+\otimes 4_1^+]$	2.560	$78\%[2_2^+]_{\rm RPA}$ $+5.8\%[2_1^+\otimes 4_1^+]$
2_3^+	2.799	2.808	$78.6\%[2_3^+]_{\rm RPA}$ $+1.7\%[2_1^+\otimes 4_2^+]$	2.808	$78.6\%[2_3^+]_{\rm RPA}]$ $+1.7\%[2_1^+\otimes 4_2^+]$
2_5^+	3.426	3.323	$20.9\%[2_5^+]_{\rm RPA}$ $+51.9\%[2_1^+\otimes 2_1^+]$	3.323	$21.1\%[2_5^+]_{\rm RPA}$ $+51.9\%[2_1^+\otimes 2_1^+]$
3_1^-	1.810	1.809	$93.7\%[3_1^-]_{\rm RPA}$ $+3.4\%[2_1^+\otimes 3_1^-]$	1.809	$93.8\%[3_1^-]_{\rm RPA}$ $+3.4\%[2_1^+\otimes 3_1^-]$
4_1^+	2.191	2.136	$94.2\%[4_1^+]_{\rm RPA}$ $+2\%[4_1^+\otimes 4_1^+]$	2.136	$94.3\%[4_1^+]_{\rm RPA}$ $+2\%[4_1^+\otimes 4_1^+]$
4_2^+	2.588	2.637	$94.9\%[4_2^+]_{\rm RPA}$	2.638	$95\%[4_2^+]_{\rm RPA}$

Several $E2$ transitions in ^{144}Sm are compared with the corresponding experimental values in Table 5. The structure of the quadrupole-quadrupole two-phonon state (denoted 2_{22}^+ in Table 5) is given in Table 4 (the two-phonon state is in fact the 2_5^+ excited state). The states with an index (23) (see the caption of Table 5) have a large two-phonon quadrupole-octupole component. The $[2_1^+\otimes 3_1^-]_{J^\pi}$ component exhausts from 82% to 95% of the norm of the wave function of the states members of the quadrupole-octupole multiplet. The calculated reduced transition probabilities for ^{140}Ce are compared with the measured ones in Table 11. The data from the nanosecond lifetime measurements are taken from Ref. 15.

The calculations and comparison with the experimental data allow one to conclude that the structure of the low-lying excited states in $N=82$ nuclei is relatively simple in the sense that only a single component is dominant. This is due to the relatively weaker quasiparticle-phonon interaction for semimagic nuclei.

Table 5. $E2$ **transition properties of several states in** ^{144}**Sm calculated in QPM. The notations** λ^{+}_{22} **and** λ^{-}_{23} **are used for the states belonging to the quadrupole-quadrupole (22) and quadrupole-octupole (23) multiplets**

I^π	J^π	$B(E2; I^\pi \to J^\pi)$[W.u.]	
		Exp.	QPM
2^+_{22}	2^+_1	-	11.4
4^+_{22}	2^+_1	-	8.1
1^-_{23}	3^-_1	16.6(40)$^{(a)}$	13.7
2^-_{23}	3^-_1	$7.8(^{+6.6}_{-5.1})^{(b)}$	10.7
3^-_{23}	3^-_1	$5.5(^{+5.7}_{-5.5})^{(b)}$	10.8
4^-_{23}	3^-_1	$4.8(^{+2.9}_{-2.6})^{(b)}$	11.6
5^-_{23}	3^-_1	$8.6(^{+11.6}_{-4.8})^{(b)}$	12.9

[a]Taken from Ref. 54

[b]Taken from Ref. 79.

Let us consider the structure of the low-lying states in ^{144}Nd obtained in RPA. The main characteristics of several of them are given in Table 6. For the collective $[2^+_1]_{\rm RPA}$ state the largest neutron RPA forward amplitude comes from the $[2f_{7/2}]^2$ two-quasiparticle component. The structure of ^{144}Nd was studied in detail in the framework of the Cluster Vibrator Model (CVM) [31]. This $[2f_{7/2}]^2$ component is important also in the structure of the neutron $\boldsymbol{d}$-boson obtained by means of a mapping procedure in the CVM [31]. The next large contribution in the CVM comes from the $[2f_{7/2}2p_{3/2}]$ neutron configuration and has nearly the same amplitude as the $[2f_{7/2}]^2$ component. In our calculations, the $[2f_{7/2}2p_{3/2}]$ two-quasiparticle component has at least a three times smaller contribution to the $[2^+_1]_{\rm RPA}$ state than the corresponding contribution to the neutron $\boldsymbol{d}$-boson in the CVM. The smaller contribution of $[2f_{7/2}2p_{3/2}]$ in comparison with the $[2f_{7/2}]^2$ component seems to be in agreement with the experimental data given in Ref. 32. This discrepancy between the two models comes mainly from the different single-particle level spacing used in the calculations. For ^{144}Nd, the $[2^+_1]_{\rm RPA}$ state is very collective and has 55% and 45% contributions from neutron and proton two-quasiparticle components, respectively. The contributions of the neutrons and the protons in the structure of the $[2^+_2]_{\rm RPA}$ state in ^{144}Nd state are 60% and 40%, respectively, and the smaller $B(E2; \text{g.s.} \to [2^+_2]_{\rm RPA})$ shows that this state is considerably less collective than the $[2^+_1]_{\rm RPA}$ state (see Table 6). The main neutron components of the $[2^+_2]_{\rm RPA}$ state have signs opposite to those of the proton ones. This means that the $[2^+_2]_{\rm RPA}$ state exhibits an isovector origin in contrast to the $[2^+_1]_{\rm RPA}$ state. This property will be discussed more quantitatively in the next section.

Table 6. Structure of the first RPA phonons (only the largest components are given) in ^{144}Nd

λ_i^π	$\omega_{\lambda_i^\pi}$[MeV]	Structure	$B(E\lambda)\uparrow[e^2b^2]$
2_1^+	0.998	$0.77\nu[2f_{7/2}]^2 + 0.55\pi[2d_{5/2}]^2$	0.48
		$0.22\nu[2f_{7/2}3p_{3/2}] + 0.45\pi[1h_{11/2}]^2$	
		$0.19\nu[1h_{11/2}2f_{7/2}] + 0.39\pi[1g_{7/2}]^2$	
2_2^+	1.997	$-1.09\nu[2f_{7/2}]^2 + 0.65\pi[2d_{5/2}]^2$	0.03
		$-0.12\nu[1i_{13/2}]^2 + 0.35\pi[1g_{7/2}]^2$	
		$-0.06\nu[2f_{7/2}3p_{3/2}] + \pi[1h_{11/2}]^2$	
4_1^+	1.780	$1.1\nu[2f_{7/2}]^2 + 0.48\pi[2d_{5/2}]^2 - 0.3\pi[1g_{7/2}2d_{5/2}]$	0.06

The parameters for the J^π=4^+ states in RPA are fixed so that the $[4_1^+]_{\rm RPA}$ state is not a pure two-quasiparticle state, although the main component is the neutron $[2f_{7/2}]^2$ (75 %–85 %). Small admixtures of two-quasiparticle proton configurations ($\sim$ 3–6 %) are also present. This structure is in agreement with the experimental results from Ref. 26.

The wave function structure (6) of the first three quadrupole states in ^{144}Nd is given in Table 7. The corresponding calculated electromagnetic transitions for ^{144}Nd are given in Table 8. The comparison with the experimental data shows a satisfactory agreement. The obtained results are in average similar to those of Refs. 31,33 for ^{144}Nd.

The first 2^+ state is predominantly a one-phonon collective state. The contribution of the one-phonon component gives 88.7% in the norm of the wave function. The second 2^+ state has a large two-phonon component (61%). This causes the strong $E2$ transition to the first 2^+ state. The strength of the $[2_2^+]_{\rm RPA}$ state, due to the quasiparticle-phonon interaction of QPM (see eq. (44)), is fragmented mainly over the 2_2^+ and 2_3^+ states (see Table 7).

The 4_1^+ and 4_2^+ states share the one-phonon $[4_1^+]_{\rm RPA}$ component and the two-phonon quadrupole-quadrupole $[2_1^+ \otimes 2_1^+]_{4^+}$ component. According to Ref. 26, the 4_1^+ state should have a collective one-phonon component, two-quasiparticle components and a two-phonon component to explain the large $B(E4)$ value (12 W.u.). We can see from Table 7 that the 4_1^+ state has a large one-phonon component ($\sim$ 66 %) and a considerable two-phonon component ($\sim$ 24 %). In this sense, our results are in agreement with the results of Ref. 26. The experimental $B(E2; 4_1^+ \to 2_1^+)$ values are also well reproduced (see Table 8). To complete our discussion on the 4_1^+ state, we should say that the $\boldsymbol{g}$-boson obtained by means of a mapping procedure in the framework of CVM [31] is much more collective

Table 7. Energies and structure of the first 2^+ and 4^+ states in ^{144}Nd. Only the main and larger than 0.1% components are presented

State	Exp.	QPM with 3 ph.		QPM without 3 ph.	
	E [MeV]	E [MeV]	Structure [%]	E [MeV]	Structure [%]
2_1^+	0.697	0.709	$88.7\%[2_1^+]_{\rm RPA}$ $+6\%[2_1^+ \otimes 4_1^+]$ $+0.1\%[[2_1^+ \otimes 2_1^+]_1 \otimes 2_1^+]$	0.714	$89.2\ \%\ [2_1^+]_{\rm RPA}$ $+6\ \%\ [2_1^+ \otimes 4_1^+]$
2_2^+	1.561	1.731	$30\%[2_2^+]_{\rm RPA}$ $+61\%[2_1^+ \otimes 2_1^+]$ $+1.8\%[[2_1^+ \otimes 2_1^+]_4 \otimes 4_1^+]$	1.772	$43.7\ \%\ [2_2^+]_{\rm RPA}$ $+\ 48.4\ \%\ [2_1^+ \otimes 2_1^+]$
2_3^+	2.066	1.999	$58.9\%[2_2^+]_{\rm RPA}$ $+27\%[2_1^+ \otimes 2_1^+]$ $+1.4\%[[2_1^+ \otimes 2_1^+]_4 \otimes 4_1^+]$	2.039	$47.6\%[2_2^+]_{\rm RPA}$ $+43.8\%[2_1^+ \otimes 2_1^+]$
4_1^+	1.311	1.464	$66.2\%[4_1^+]_{\rm RPA}$ $+23.6\%[2_1^+ \otimes 2_1^+]$ $+0.4\%[[2_1^+ \otimes 2_1^+]_1 \otimes 2_1^+]$	1.510	$73.9\%[4_1^+]_{\rm RPA}+$ $+18\%[2_1^+ \otimes 2_1^+]$
4_2^+	2.109	1.965	$16.8\%[4_2^+]_{\rm RPA}$ $+60.6\%[2_1^+ \otimes 2_1^+]$ $+1.8\%[[2_1^+ \otimes 2_1^+]_4 \otimes 4_1^+]$	2.010	$15.1\%[4_1^+]_{\rm RPA}$ $+66.6\%[2_1^+ \otimes 2_1^+]$
4_3^+	2.295	2.219	$57.6\%[4_2^+]_{\rm RPA}$ $+11.7\%[2_1^+ \otimes 2_1^+]$ $+4\%[[2_1^+ \otimes 2_1^+]_1 \otimes 2_1^+]$	2.250	$66.5\%[4_2^+]_{\rm RPA}$ $+11.3\%[2_1^+ \otimes 2_1^+]$

than our $[4_1^+]_{\rm RPA}$ state. To determine unambiguously the structure of the 4_1^+ state more precise experimental information is needed for more nuclei from this region.

The 4_3^+ state is a noncollective one. The structure of the lowest three 4^+ states is similar for the other investigated nuclei. It was observed that the 4_2^+ state (1.965 MeV) feeds the 2_1^+ state appreciably while the 4_3^+ state (2.219 MeV) feeds very weakly the 2_1^+ state.

The structure of the excited states in the $N = 84$ nuclei is more complicated than those of the semimagic ones. The reason is the larger quasiparticle-phonon interaction and the smaller energy difference between the basic states. The influence of the three-phonon components has been found to be significant.

Table 8. Electromagnetic properties of several positive parity states in ^{144}Nd calculated in QPM

I^π	Energy [keV]		λ	J^π	$B(E\lambda; I^\pi \to J^\pi)[e^2fm^{2\lambda}]$	
	Exp.	QPM			Exp.	QPM
2_1^+	696.5$^{(b)}$	709	E2	0_1^+	1.08×10$^{3(a)}$	0.72×10^3
2_2^+	1561$^{(c)}$	1731	E2	0_1^+	0.001(1)×10$^{4(e)}$	0.002
	864.5	1022	E2	2_1^+	0.95(21)×10$^{3(e)}$	1.2×10^3
2_3^+	2073$^{(c)}$	1999	E2	0_1^+	0.45×10$^{2(a)}$	0.73×10^2
	1376.5	1290	E2	2_1^+	2(1)×10$^{2(e)}$	4×10^2
3_1^-	1510.7$^{(b)}$	1527	E3	0_1^+	2.86×10$^{4(a)}$	3.38×10^4
4_1^+	1315$^{(c)}$	1464	E4	0_1^+	4.3×10$^{5(d)}$	4.1×10^5
	618.5	755	E2	2_1^+	8(1)×10$^{2(e)}$	7.6×10^2
					$Q_2\left[2_1^+\right]$ $[eb]$	
					Exp.	QPM
					-39(21)$^{(e)}$	-22

[a] Taken from Ref. 26.
[b] Taken from Ref. 80.
[c] Taken from Ref. 81.
[d] Taken from Ref. 82.
[e] Taken from Refs. 31,33.

4. THE LOW-LYING ISOVECTOR MODE

The low-lying quadrupole states in the N =84 isotones have been subjected to several experimental and theoretical investigations in connection with the so-called isovector or mixed-symmetry states [29-39]. The small mixing ratios $\delta(E2/M1; 2_3^+ \to 2_1^+)$ and relatively large value of $B(M1; 2_3^+ \to 2_1^+)$ correspond to a classification of the first 2^+ state as a symmetric state and of the third 2^+ state as a mixed-symmetry state in the $U(5)$-limit of IBM-2 [34, 35]. In the frame of the extended vibrational model [36], the isospin dependence of the collective coordinates is used and the 2_1^+ state is regarded as an in-phase (isoscalar) vibration and the 2_3^+ as an out-of-phase (isovector) vibration of protons and neutrons. The vibrational model described the characteristic features (energies and multipole mixing ratios) of low-lying 2^+ states observed experimentally, in nuclei near the shell closures (^{124}Te, ^{140}Ba, ^{142}Ce and ^{144}Nd). Other theoretical efforts to understand the origin of the low-lying quadrupole states in this region have been undertaken in the framework of the shell model [37] as well as in the pairing-plus-

quadrupole model [38]. The properties of the $M1$ transitions between low-lying states and their theoretical interpretation are reviewed in Ref. 39.

In Ref. 33, a detailed calculation for the $N = 84$ isotones has been performed using the two-Particle-core Coupling Model (PCM) and IBM-2 in order to study the validity of the interacting boson model in these nuclei. A general mapping procedure between the obtained wave functions in both models has been proposed and applied for ^{144}Nd. Although both models give a reasonable description of the excited states' energies, differences occur in the electromagnetic decay probabilities. For instance, the IBM-2 fit fails to reproduce both the $B(E2; 2_3^+ \to$ g.s.) and the $B(M1; 2_3^+ \to 2_1^+)$ values. It predicts as well, in contradiction to the experiment, that the $B(E2; 4_1^+ \to 2_1^+)$ value should be a factor of 1.4 times larger than the $B(E2; 2_1^+ \to$ g.s.) value. The PCM gives reasonable agreement for all these quantities. Both models could not reproduce the signs of the $\delta(E2/M1; 2_3^+ \to 2_1^+)$ and $\delta(E2/M1; 2_2^+ \to 2_1^+)$ mixing ratios.

The experimental data, obtained by direct lifetime measurements [40], show that the $B(M1; 2_3^+ \to 2_1^+)$ value in ^{144}Nd is close to the value of the single particle estimation for this transition. This means that the low-lying states in ^{144}Nd contain significant two-particle components. Considering the relative sign of the main neutron and proton components, the $[2_1^+]_{\rm RPA}$ state is a symmetric and the $[2_2^+]_{\rm RPA}$ state is an antisymmetric state (see Table 6). A relevant quantity [41] to check the nature of a RPA phonon, taking into account its structure, is the ratio:

$$B = \frac{|\langle 2_i^+ \| \sum_k^{\rm p} {\rm r}_k^2\, Y_{2\mu}(\Omega k) - \sum_k^{\rm n} {\rm r}_k^2\, Y_{2\mu}(\Omega k) \| {\rm g.s.}\rangle|^2}{|\langle 2_i^+ \| \sum_k^{\rm p} {\rm r}_k^2\, Y_{2\mu}(\Omega k) + \sum_k^{\rm n} {\rm r}_k^2\, Y_{2\mu}(\Omega k) \| {\rm g.s.}\rangle|^2}. \qquad (12)$$

As shown in Ref. 41, in the case of $B > 1$, the 2^+ state under consideration is an isovector state, otherwise an isoscalar one. As shown in Table 9, in our results, the $[2_1^+]_{\rm RPA}$ state is an isoscalar state and the $[2_2^+]_{\rm RPA}$ state an isovector one.

Table 9. Values of the quantity B (see eq.(12)) for ^{140}Ba, ^{142}Ce, ^{144}Nd and ^{146}Sm

		B			
Nucl.		^{140}Ba	^{142}Ce	^{144}Nd	^{146}Sm
State	2_1^+	0.0003	6×10^{-5}	10^{-5}	2×10^{-5}
	2_2^+	25.6	10.1	3.4	5.3

Table 10. Some results in QPM compared with experimental data in different N = 82 nuclei

Nuclei	Quantity	Exp.	QPM
^{138}Ba	$B(E2;2_1^+ \to 0_1^+)[e^2b^2]$	$0.0452\pm0.0018^{(a)}$	0.050
	$B(E3;0_1^+ \to 3_1^-)[e^2b^3]$	$0.133\pm0.013^{(b)}$	0.115
	$E_{3_1^-}$[MeV]	$2.881^{(e)}$	2.907
^{140}Ce	$B(E2;2_1^+ \to 0_1^+)[e^2b^2]$	$0.061\pm0.020^{(c)}$	0.068
	$B(E3;0_1^+ \to 3_1^-)[e^2b^3]$	$0.21\pm0.03^{(b)}$	0.147
	$E_{3_1^-}$[MeV]	$2.465^{(e)}$	2.345
^{142}Nd	$B(E2;2_1^+ \to 0_1^+)[e^2b^2]$	$0.0562\pm0.0002^{(d)}$	0.065
	$B(E3;0_1^+ \to 3_1^-)[e^2b^3]$	$0.2620\pm0.0015^{(d)}$	0.226
	$E_{3_1^-}$[MeV]	$2.083^{(e)}$	1.973
^{144}Sm	$B(E2;2_1^+ \to 0_1^+)[e^2b^2]$	$0.0532\pm0.0016^{(a)}$	0.046
	$B(E3;0_1^+ \to 3_1^-)[e^2b^3]$	$0.27\pm0.05^{(b)}$	0.3
	$E_{3_1^-}$[MeV]	$1.810^{(e)}$	1.718

[a]Taken from Ref.57.
[b]Taken from Ref.29.
[c]Taken from Ref.83.
[d]Taken from Ref.28.
[e]Taken from Ref.27.

As already mentioned, in ^{144}Nd, there is a fragmentation of the $[2_2^+]_{\rm RPA}$ isovector state over the 2_2^+ and 2_3^+ states (see Table 7). Because of this fragmentation the large $M1$ transition strength between the $[2_1^+]_{\rm RPA}$ and the $[2_2^+]_{\rm RPA}$ states will be shared by the transitions from the 2_2^+ and 2_3^+ states to the 2_1^+ state. A similar behaviour of the $M1$ fragmentation is discussed in Ref. 39. According to the QPM calculations, there are five 2^+ RPA states below 3 MeV. The value of the quantity $\sum_i B(M1;[2_i^+]_{\rm RPA} \to [2_1^+]_{\rm RPA})$ is equal to 0.64 μ_N^2. The main contribution in this sum comes from the $B(M1;[2_2^+]_{\rm RPA} \to [2_1^+]_{\rm RPA})$ value, which is 50 times larger than the other terms. The proton orbital part of it is about 70%. The latter is in qualitative agreement with shell model calculations for medium mass spherical nuclei [42]. The quasiparticle-phonon interaction distributes about 90 % from the total RPA $M1$ strength over seven excited states under 3 MeV. Because of the dominance of the $B(M1;[2_2^+]_{\rm RPA} \to [2_1^+]_{\rm RPA})$, which is mainly due to proton orbital contributions (see the discussion above), the main part in

the distribution comes from the proton orbital $M1$ term. The latter feature of the $M1$ transition between the low-lying states is discussed in detail in Ref. 43.

Table 11. Some reduced transitions probabilities rates in ^{140}Ce

	Exp.	QPM
$B(E2;2_1^+ \to 0_1^+)$ $[e^2b^2]$	$0.061 \pm 0.020^{(d)}$	0.068
$B(E2;2_2^+ \to 0_1^+)$ $[e^2b^2]$	$\geq 6.8 \times 10^{-7(a)}$	0.001
$B(E2;2_2^+ \to 2_1^+)$ $[e^2b^2]$	$\geq 1.2 \times 10^{-4(a)}$	0.0056
$B(M1;2_2^+ \to 2_1^+)$ $[\mu_N^2]$	$\geq 3.4 \times 10^{-4(a)}$	0.044
$B(E2;4_1^+ \to 2_1^+)$ $[e^2b^2]$	$(6.2 \pm 0.4) \times 10^{-4(a)}$	12.3×10^{-4}
$B(E2;2_3^+ \to 4_1^+)$ $[e^2b^2]$	$(1.5 \pm 0.7) \times 10^{-4(b)}$	5.6×10^{-4}
$B(E2;6_1^+ \to 4_1^+)$ $[e^2b^2]$	$(1.1 \pm 0.3) \times 10^{-3(d)}$	1.5×10^{-3}
$B(E3;3_1^- \to 0_1^+)$ $[e^2b^3]$	$0.0300 \pm 0.0043^{(c)}$	0.021
$\delta(E2/M1;2_2^+ \to 2_1^+)$	$0.37 \pm 0.06^{(e)}$	0.2

[a] Taken from Ref.15.
[b] Taken from Ref.57.
[c] Taken from Ref.29.
[d] Taken from Ref.83.
[e] Taken from Ref.84.

Table 12. Comparison of QPM calculations with experimental $M1$ transitions and δ ratios in ^{144}Nd

	Exp.	QPM
$B(M1;2_2^+ \to 2_1^+)(\mu_N^2)$	$0.11^{(a)}$	0.13
$B(M1;2_3^+ \to 2_1^+)(\mu_N^2)$	$0.14(0.04)^{(a)}$	0.32
$\delta(E2/M1;2_2^+ \to 2_1^+)$	$-1.13(22)^{(b)}$	-1.02
$\delta(E2/M1;2_3^+ \to 2_1^+)$	$0.31(11)^{(b)}$	0.43

[a] Taken from Ref. 31,33.
[b] Taken from Ref. 40.

The calculated $B(M1)$ values and the mixing ratios for ^{144}Nd are given in Table 12. The obtained results are in average similar to those of Refs. 31,33 for ^{144}Nd. With respect to the structure of the 2_2^+ and 2_3^+ states, relevant quantities are: the mixing ratios $\delta(E2/M1;2_2^+ \to 2_1^+)$ and $\delta(E2/M1;2_3^+ \to 2_1^+)$ and the corresponding $B(M1)$ transition values. The higher value of the $B(M1;2_3^+ \to 2_1^+)$ compared to that of the $B(M1;2_2^+ \to 2_1^+)$ is reproduced in our calculations.

This means that the fragmentation of the $[2_2^+]_{\mathrm{RPA}}$ isovector state over the excited states is realistic. Taking into account the structure of the $[2^+]_{\mathrm{RPA}}$ states and the final distribution of these states we can conclude that the first 2^+ state is of isoscalar type and the third 2^+ state of mixed (isoscalar and isovector) type, although with a main isovector component (59 %). It should be noted that the mixing ratio δ differs (sometimes by a factor of 2) in different experiments [27, 40, 44].

5. COMPARISON OF THE QPM AND THE IBM APPROACHES

In this section, we shall consider the comparison between the description of the structure of the low-lying states in ^{146}Sm in IBM-2 [45] and in QPM. Several IBM studies in the Sm isotopes' region have been published. The nucleus ^{146}Sm has been treated in Refs. 46,47. The IBM results used here are taken from Ref. 13.

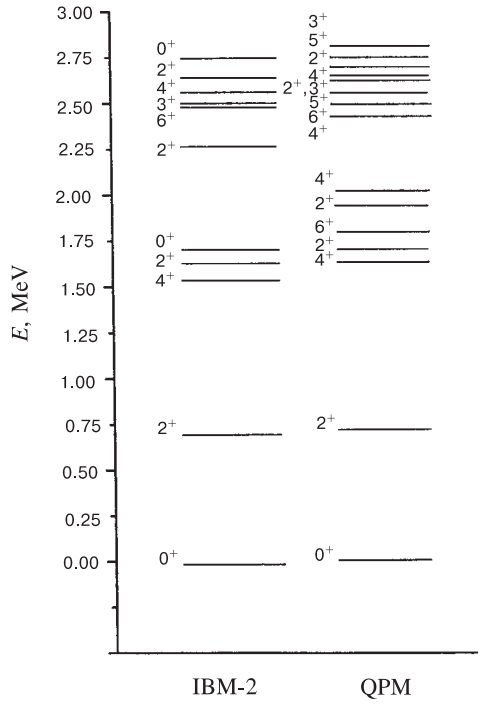

Fig. 4. Comparison of the ^{146}Sm positive parity energy levels in IBM-2 and QPM

The obtained results, in both models, for the energies and the structure of the excited states with J^π=2^+ and 4^+ in ^{146}Sm are shown in Tables 13-17, the calculated energy distribution of all positive parity states is plotted in Fig.4. The QPM states with excitation energy below 2 MeV are mainly constituted of collective components. For the first 2^+ state, the main component arises from the $[2_1^+]_{\rm RPA}$ phonon. In the structure of the 2_2^+ and 4_1^+ states, the two phonon component $[2_1^+ \otimes 2_1^+]_{J^\pi}$ is the most important. The calculated energies and $B(E2)$ values, involving the states below 2 MeV, are in good agreement with the experimental data.

Table 13. Energies and structure of the lowest three 2^+ and 4^+ excited states in ^{146}Sm, calculated in the framework of the QPM. Only the main components of the wave function are given

I_i^π	$E_{\rm exp.}$[MeV]	$E_{\rm cal.}$[MeV]	Structure
2_1^+	0.747	0.737	$91\%[2_1^+]_{\rm RPA}$
2_2^+	1.647	1.672	$75\%\left[[2_1^+]_{\rm RPA} \otimes [2_1^+]_{\rm RPA}\right] + 14\%[2_2^+]_{\rm RPA}$
2_3^+	2.155	1.944	$79\%[2_2^+]_{\rm RPA} + 11\%\left[[2_1^+]_{\rm RPA} \otimes [2_1^+]_{\rm RPA}\right]$
4_1^+	1.381	1.616	$45\%[4_1^+]_{\rm RPA} + 48\%\left[[2_1^+]_{\rm RPA} \otimes [2_1^+]_{\rm RPA}\right]$
4_2^+	2.280	2.042	$49\%[4_1^+]_{\rm RPA} + 39\%\left[[2_1^+]_{\rm RPA} \otimes [2_1^+]_{\rm RPA}\right]$
4_3^+	2.439	2.502	$96\%[4_2^+]_{\rm RPA}$

Table 14. Comparison of experimental, IBM and QPM results for some $B(E2)$ values among collective states in ^{146}Sm

	$B(E2)$ $[e^2b^2]$		
$I_i \to I_f$	Exp. [85]	IBM	QPM
$2_1^+ \to 0_1^+$	> 0.033	0.069	0.069
$4_1^+ \to 2_1^+$	> 0.06	0.108	0.093
$6_1^+ \to 4_1^+$	$0.043^{+0.054}_{-0.023}$	-	0.01

Most of the QPM states with excitation energy above 2 MeV are of noncollective nature. Some of them have large two-phonon and three-phonon components. The structure of some states is quite complicated and is exhausted by several components. It should be noted that the three-phonon components are distributed over several levels. The number of levels below 3.5 MeV is well reproduced and only for a few levels the discrepancy between the calculated and measured energies exceeds 150 keV. A satisfactory agreement with experimental data is also

Table 15. Some reduced $E2$ transition probabilities in ^{146}Sm, calculated in the QPM

$B(E2)$	
$I_i \to I_f$	$[e^2b^2]$
$2_2^+ \to 0_1^+$	0.0031
$2_3^+ \to 0_1^+$	0.0093
$2_4^+ \to 0_1^+$	0.0005
$2_2^+ \to 2_1^+$	0.12
$2_3^+ \to 2_1^+$	0.04
$2_4^+ \to 2_1^+$	0.0001
$4_2^+ \to 2_1^+$	0.07
$4_3^+ \to 2_1^+$	0.001

Table 16. Comparison of experimental, IBM and QPM results for some $E2$ transition ratios in ^{146}Sm. The experimental data is taken from Ref. 13

$\frac{I_i \to I_f}{I_i \to I_{f'}}$	$\frac{B(E2;I_i \to I_f)}{B(E2;I_i \to I_{f'})}$		
	Exp.	IBM	QPM
$\frac{2_2^+ \to 2_1^+}{2_2^+ \to 0_1^+}$	74±30	84	40
$\frac{2_3^+ \to 2_1^+}{2_3^+ \to 0_1^+}$	9÷18	9.6	4.1
$\frac{4_2^+ \to 2_1^+}{4_2^+ \to 4_1^+}$	0.7÷2.0	1.4	1.8
$\frac{2_4^+ \to 2_1^+}{2_4^+ \to 0_1^+}$	< 1.5	0.30	0.2

achieved for the reduced $E2$ transition probabilities (see Tables 14 and 16). The results obtained within the QPM and within the IBM display some differences as well as some common features. This arises from the physical backgrounds of both models. The IBM model, in the version including protons and neutrons (IBM-2) in its model space, has combinations of bosons roughly corresponding to the $[2_1^+]_{\rm RPA}$ isoscalar phonon and to the $[2_2^+]_{\rm RPA}$ isovector phonon in the language of the QPM. The good agreement between the IBM and the QPM is thus observed for QPM states involving collective components. On the other hand, the lowest 6^+ state of ^{146}Sm in the IBM is to be expected at an excitation energy $E \geq 3E(2_1^+)$ (≈ 2.4 MeV). The energy of the 6_1^+ state calculated in the QPM is E=1.744 MeV. This state is of noncollective character, as is suggested also from a smaller $B(E2, 6_1^+ \to 4_1^+)$ value in comparison with the $B(E2; 4_1^+ \to 2_1^+)$ value (see Table 14). The properties of the 6_1^+ state in ^{146}Sm, calculated within

Table 17. Comparison of experimental, IBM and QPM results for some mixing ratios ($\delta(E2/M1)$) in ^{146}Sm

	$\delta(E2/M1)$		
$I_i \to I_f$	Exp.	IBM	QPM
$2_2^+ \to 2_1^+$	$-2.2^{(a)}$	-2.13	-1.3
$2_3^+ \to 2_1^+$	-3.2$\leq \delta \leq -0.9^{(b)}$	0.059	0.4

[a] Taken from Ref.44.

[b] Taken from Ref.46.

the QPM, agree with the experimental data. The QPM predicts a collective three-phonon 6^+ state at excitation energy of 2.62 MeV, which is in agreement with the IBM lowest 6^+ state energy.

The energy of the 4_1^+ level is lower than twice the energy of the 2_1^+ state. This fact is pointing out that components different from the two-phonon quadrupole collective one are important in its structure. In the QPM calculations, the $[2_1^+ \otimes 2_1^+]_{4^+}$ two-phonon component is shared by the 4_1^+ and 4_2^+ states. The latter contain an important $[4_1^+]_{\rm RPA}$ component as well. This is the reason for the nearly equal QPM $E2$ transition probabilities between the first two 4^+ states and the 2_1^+ state (Table 15). The importance of the $[4_1^+]_{\rm RPA}$ component in the QPM 4^+ states suggests that a better description within the IBM framework could be achieved by enlarging the IBM model space so as to include also the L=4 **g**-boson.

In the IBM, the decay of the 4_2^+ state to the 2_1^+ state is suppressed. Such suppression is observed for the third 4^+ state (2.439 MeV) in the experimental spectrum. In the QPM, the 4_3^+ state in ^{146}Sm is a noncollective state, which leads to a very small $B(E2, 4_3^+ \to 2_1^+)$ value (see Table 15).

In Table 17, results are given for some mixing ratios δ in ^{146}Sm. We must note that the experimental information is quite indeterminate. The results of both calculations, in the QPM and in the IBM, also differ appreciably. The noncollective components have an important influence on the QPM δ values. A qualitative agreement of the two models occurs only in the cases when in the structure of the initial and final states the contribution from the collective components (one- and two-phonon ones) is large ($2_2^+ \to 2_1^+; 2_3^+ \to 2_1^+$). Further study along this line would be fruitful only if more precise experimental information is available.

The 2_3^+ state (E=2.156 MeV) in ^{146}Sm is interpreted as an isovector state in both models. The quite uncertain experimental information does not contradict this interpretation.

6. ELECTRIC DIPOLE TRANSITIONS IN THE $N = 82$ AND THE $N = 84$ ISOTONES

Recently, the interest in low-lying vibrations in nuclei has increased considerably with the appearance of experimental evidences for two-phonon quadrupole-octupole and octupole-octupole excitations in the semimagic $N = 82$ nuclei [46-53]. In Ref. 49, the $B(E1)$ value from the first 1^- state to the ground state has been measured in ^{144}Sm, using the nuclear resonance fluorescence method. It is suggested in Ref. 49 that this 1^- state might be a member of the two-phonon quadrupole-octupole multiplet expected at this energy. Earlier measurements of the $E1$ transition between the first 3^- and 2^+ states were reported in Ref. 48, where an $(\alpha\alpha')$ Coulomb excitation study has been performed in the same nuclei. The comparison of the obtained $B(E1; 2^+_1 \rightarrow 3^-_1)$ with the $B(E1; 1^-_1 \rightarrow \text{g.s.})$ value also supports the two-phonon structure of the 1^-_1 state. In Refs. 50,51, ^{144}Sm has been investigated via the $(n, n'\gamma)$ reaction and a large number of fast ($> 10^{-3}$W.u.) $E1$ transitions has been observed. The typical rates for the $E1$ transitions, known from systematics, are of the order of 10^{-4}—10^{-8} W.u. [56,57]. The larger values of the recently reported $B(E1)$ transitions reveal that the corresponding states have a different origin than those reported in Refs. 56,57. However, as shown in Ref. 51, the enhanced $E1$ transitions are typical for the N =82 nuclei [53].

A description of the properties of the quadrupole-octupole and octupole-octupole multiplets has been proposed in Ref. 58. Later on, calculations have been performed in the frame of the QPM, studying the first dipole states in many spherical nuclei [59]. Within the same model, $E1$ transitions have been calculated in deformed nuclei [60]. A description of some members of the octupole two-phonon multiplets in the framework of the **spdf** IBM has been given in Ref. 61. The interplay of different shells in the $E1$ transitions has been discussed in Ref. 62. The first 1^- state has been described as a $2^+_1 \otimes 3^-_1$ two-boson state in the IBM [48]. The theoretical investigations show that the first 1^- state has an isoscalar character. The latter is a hint that the large $B(E1)$ values, obtained recently, may be the result of a the interplay between isoscalar and isovector modes in the structure of the low-lying excited states. Theoretical and experimental investigations for ^{144}Sm have been performed in Ref. 63. In this paper, high-resolution (p, p') analysis has been used to derive information about the character of the transitions involving the presumed members of the two-phonon octupole multiplets. In the same paper, the available experimental information concerning the $E1$ transitions in ^{144}Sm has been compared to nuclear field theory calculations. This investigation confirms the two-phonon character of the states pointed out in Ref. 50, although some mixing with two-quasiparticle components has been found. A direct experimental evidence for the two-phonon nature of the first dipole state in ^{144}Sm has been obtained in Ref. 54, where a

good agreement with a previous prediction for the $B(E2; 1_1^- \to 3_1^-)$ value, given within the QPM [16], has been observed (see Table 5).

The $E1$ transitions at low energy in atomic nuclei are strongly hindered. The reason for this hinderance is manifold: the isoscalar part of the $E1$ operator should not contribute to the $E1$ transition; the isovector $E1$ interaction is repulsive and shifts the $E1$ strength to higher excitation energies; the pairing factor involved in the $E1$ transition operator, which does not change the number of quasiparticles (see eq. (9)), should be much smaller than unity; the $E1$ matrix element between the main components of the wave functions is often very small or vanishes at low energy. The reduction due to the isovector channel of the interaction may be expressed as an effective charge for the $E1$ transition [1]. The expression reads:

$$e_{\text{eff}} = e(1 + \chi).$$

Adding the correction for the center of mass motion the above equation becomes:

$$e_{\text{eff}} = -\frac{1}{2}e(\tau_z - \frac{N - Z}{A})(1 + \chi). \tag{13}$$

The parameter χ has been qualitatively estimated to be approximately equal to -0.7 in Ref. 1. Determination of χ via comparison with experiment for some nuclei has been done in Ref. 64.

The appropriate nuclear model to study the properties of the low-lying 1^- states must possess two main features. The first one is to incorporate the Giant Dipole Resonance (GDR) which means to deal with a large single-particle space and a sufficiently complex interaction. The second is the detailed reproduction of the two-phonon states' fragmentation, which requires that the collective basis of the model should include at least up to three-phonon states.

In the case of the 1^- states the matrix element mixing the GDR and the low-lying $[2_1^+ \otimes 3_1^-]_{1^-}$ state reads (see eq. (45)):

$$U_{2_1^+}^{3_1^-}(GDR) = \left\langle Q_{1^-GDR} \left| H_{int} \right| \left[Q_{2_1^+}^+ Q_{3_1^-}^+ \right]_{1^-} \right\rangle. \tag{14}$$

Because of the isovector origin of the GDR, the neutron and proton components of the wave function (6) contribute with opposite signs in (14) and it becomes small [3, 59]. A serious test for a model would be to predict not only the magnitude of the matrix element (14) but also its sign. It must be stressed that in the present case a very weak $E1$ transition ($\approx$ 3mW.u.) has to be described, taking into accout the influence of the GDR ($\approx$ 10W.u.).

We have applied the model to study the properties of the low-lying 1^- states in N =82 and N =84 isotones. The results for ^{144}Sm and ^{144}Nd are compared with the available experimental information in Table 18. It is seen from Table 18 that the calculated structure of the 1_1^- state is mainly a two-phonon one for ^{144}Sm

Table 18. Energies and $B(E1)$ values for the 1^-_1 state in ^{144}Sm and ^{144}Nd, compared with experimental data

	^{144}Sm		^{144}Nd	
	calc.	exp.	calc.	exp.
$E(1^-_1)$[MeV]	3.440	3.225	2.47	2.185
Structure	$95\%\left[2^+_1\otimes 3^-_1\right]$		$83\%\left[2^+_1\otimes 3^-_1\right]$ $+9\%\left[\left[2^+_1\otimes 2^+_1\right]_2\otimes 3^-_1\right]$	
$B(E1; g.s\to 1^-_1)\left[e^2fm^2\right]$	18.1×10^{-3}	$18.9\times10^{-3(a)}$	6.3×10^{-3}	$7.2\times10^{-3(b)}$
$B(E1; \text{g.s.}\to(2ph)_{1^-_1})\left[e^2fm^2\right]$	52.2×10^{-3}		51.6×10^{-3}	
$B(E1; \text{g.s.}\to(1ph)_{1^-_1})\left[e^2fm^2\right]$	8.8×10^{-3}		21.8×10^{-3}	

[a] Taken from Ref. 50.
[b] Taken from Ref. 55.

(N=82), while for the N =84 nucleus ^{144}Nd, there is a contribution from the three-phonon component ($[[2^+_1\otimes 2^+_1]_2\otimes 3^-_1]_{1^-}$). The isovector $E1$ strength is concentrated predominantly in a single RPA state (the GDR). For ^{144}Sm this RPA state collects 60% of the EWSR, while for ^{144}Nd it collects 56%. In the same time, its contribution in the wave function (6) of the 1^-_1 state is less than 0.5%.

The reduced matrix element of the $E1$ operator (see eq. (9)) between the 1^-_1 and the ground state reads:

$$\langle\Psi\,|M(E1)|\,0\rangle\sim$$
$$\sim R_{GDR}\,\langle Q_{1^-GDR}\,|M(E1)|\,0\rangle + P^{2^+_1}_{3^-_1}(1^-_1)\left\langle\left[Q_{2^+_1}Q_{3^-_1}\right]_{1^-}|M(E1)|\,0\right\rangle. \quad (15)$$

The R_{GDR} and $P^{2^+_1}_{3^-_1}$ are coefficients of the wave function (6). The contribution of the two-phonon part in (15) dominates, because of the large value of the coefficient $P^{2^+_1}_{3^-_1}$. The very small value of the coefficient R_{GDR} is multiplied by the large matrix element connected with the GDR, but the product contributes in (15) less than the two-phonon part. The corresponding reduced transition probabilities are given in Table 18. The quantity $B(E1)_{1ph}$ is connected with the GDR (first term in eq. (15)). The quantity $B(E1)_{2ph}$ is the part of the transition due to the two-phonon component of the wave function (6) (second term in eq. (15)). Both ingredients of (15) have opposite signs and the $B(E1)_{2ph}$ is largely reduced. The calculated $B(E1;\text{g.s.}\to 1^-_1)$ value is in good agreement with the experimental data in both nuclei. The calculated energies and $B(E1)$ values are compared with the experimental results in Table 19 for the $N=82$ isotones.

Table 19. Comparison of experimental data and QPM results for the two-phonon 1^- states in the $N = 82$ isotones. The experimental results are taken from Ref. 53

		^{138}Ba	^{140}Ce	^{142}Nd	^{144}Sm
$E_{1^-\text{Exp.}}$[keV]		4026	3643	3425	3225
$E_{1^-\text{QPM}}$[keV]		3582	3611	3590	3600
$B(E1; 1_1^- \to \text{g.s.})_{\text{Exp.}}$	[m W.u.]	2.5(5)	3.2(2)	3.1(5)	3.6(5)
$B(E1; 1_1^- \to \text{g.s.})_{\text{QPM}}$	[m W.u.]	2.8	3.2	3.03	3.4

The reasonable agreement between the QPM results and experiment, concerning the so subtle properties of the dipole transitions, shows that the model reproduces well the intricate interplay of isoscalar and isovector modes in the structure of the low-lying states. The properties of all states members of the quadrupole-octupole multiplet, other than the 1^- state, are discussed in detail in Ref. 16.

7. EVIDENCES FOR OCTUPOLE–COUPLED MULTIPHONON STATES IN ^{124}Te

In this section, we shall present results of the QPM compared to experimental results from various experiments investigating the nucleus ^{124}Te following Ref. 65. The structure of the even-even nucleus ^{124}Te has been the subject of considerable interest [64-70], since it is an ideal testing ground for different theoretical models. Up to now, however, no complete understanding of the nuclear structure of this isotope has been achieved. Even many aspects of the low-lying spectrum are still puzzling [71]. At lower excitation energies ^{124}Te seems to be an ideal collective nucleus. The energy ratio of the first 4^+ level to the first 2^+ level is nearly two. This supports a spherical picture, as for instance obtained in SU(5) limit of the IBM. On the other hand, the level sequences show that only the 2^+ and the 4^+ states of the two phonon triplet are in correct energy region, whereas the corresponding first 0^+ level is about 300 keV too high in excitation energy. This implies a more complex structure of the nucleus ^{124}Te which cannot be fully described by current microscopic models. In order to achieve a better understanding of these problems, one needs extensive and complete experimental information. Here, we make use of the results of a variety of experimental data, taken from Ref. 65, which were measured in different reactions, the aim being to obtain the maximum of information in order to find the largest possible correspondence with the theoretical interpretation of the structure of ^{124}Te within the QPM. A special attention is paid to the unusual de-excitation cascade in the level scheme of ^{124}Te which has been known for a long time, but never examined in

detail [73]. The suggestion is made that this unusual cascade may be related to the presence of multiphonon structures with negative parity.

The $E\lambda$ transitions have been calculated with $e^p_{\rm eff} = 1.25e$ and $e^n_{\rm eff} = 0.25e$, except for the $E1$ transitions. In the present case the effective charge is a parameter fixed to reproduce the $B(E2)$ transitions from the ground state to the first 2^+ state. The effective charges for the $E1$ transitions have to be reduced according to Refs. 1, 64 (see also the discussion in Section 6 and eq. (13)). In our calculations mixing with the GDR is taken explicitly into account and to reproduce the $B(E1)$ strength for its excitation we use the following effective charges: $e^n_{\rm eff}(E1) = -0.39e$ and $e^p_{\rm eff}(E1) = 0.53e$. They have been used to calculate all other $E1$ transitions as well.

A comparison of the experimental level scheme with the one calculated in the QPM is presented in Table 20 where additionally the largest multiphonon amplitudes are listed for collective levels. The excitation energies of dominant one- and two-phonon states are well reproduced, but generally too high for states with a large three-phonon component. This can be traced back to the omission of more complex configurations. It has to be expected that due to the interaction between phonons specific for the QPM (coupling between components differing by one phonon, see eq. (44) in the Appendix) the inclusion of four-phonon components will improve the above-mentioned deficiency.

The 0^+ state cannot be well reproduced by the theory. One would have to account for this by using strong anharmonicities [71]. The 6^+_1 state is a three-phonon quadrupole state in the calculations. However, the almost constant excitation energy experimentally observed for this level in different Te isotopes suggests a noncollective structure [74]. Thus, it would better correspond to the 6^+_2 model state, but the energy difference of 540 keV to the experiment would be rather large.

Electromagnetic transition probabilities, $E2/M1$ mixing ratios and branching ratios between low-lying collective states are compared in Table 21 to QPM results. The quadrupole moment of the 2^+_1 level and the $B(E2)$ values to the lowest 2^+ states agree well. Signs and magnitudes of $E2/M1$ mixing ratios for transitions between the lowest 2^+ states are reproduced. Also many branching ratios are reasonably described.

In order to account for the large number of experimentally observed 2^+ levels it was proposed that the fourth 2^+ state at 2.092 MeV has an isovector structure [70] (see also the discussion in Section 4). The third 2^+ state in the QPM calculation is proposed to correspond to this level. A small mixing ratio $\delta(E2/M1; 2^+_3 \to 2^+_1)$ and a large $B(M1; 2^+_3 \to 2^+_1)$ value would support such a classification [34, 35]. For ^{124}Te the calculated $\delta(E2/M1; 2^+_3 \to 2^+_1) = 0.07$ has to be compared with the experimental value of 0.13(12) [34, 70]. Moreover, the 2^+_3 level has a dominant $[2^+_2]_{\rm RPA}$ phonon contribution (81%). The comparison of the structure of this phonon in terms of two-quasiparticle components compared

Table 20. Level scheme of ^{124}Te calculated in the QPM. For the collective states the main component of the QPM wave function is given. For comparison the experimentally measured level energies are included where possible

J^π	Root number	E_{th} [MeV]	QPM wave function	[%]	$E_{exp}^{(a)}$ [MeV]
0^+	1	1.080	$2_1^+ \otimes 2_1^+$	83	1.657
0^+	2	2.085	$2_1^+ \otimes 2_1^+ \otimes 2_1^+$	50	1.883
0^+	3	2.383			2.308
1^+	1	2.749			
1^+	2	3.098			
1^+	3	3.185			
1^-	1	2.985	$2_1^+ \otimes 3_1^-$	91	2.747
1^-	2	3.796	$2_1^+ \otimes 2_1^+ \otimes 3_1^-$	70	3.092
1^-	3	4.063			
2^+	1	0.599	2_1^+	92	0.603
2^+	2	1.408	$2_1^+ \otimes 2_1^+$	87	1.325
2^+	3	1.986	$[2_2^+]_{\mathrm{RPA}}$	81	2.091
2^+	4	2.100	$2_1^+ \otimes 2_1^+ \otimes 2_1^+$	70	2.039
2^+	5	2.246			
2^+	6	2.386			
2^+	7	2.398			
2^+	8	2.610			
2^+	9	2.741			
2^-	1	3.057	$2_1^+ \otimes 3_1^-$		92
2^-	2	3.302			
2^-	3	3.770	$2_1^+ \otimes 2_1^+ \otimes 3_1^-$	42	3.101
3^+			$2_1^+ \otimes 2_1^+ \otimes 2_1^+$	90	
3^+					
3^-	1	2.277	3_1^-	79	2.294
3^-	2	2.781	$2_1^+ \otimes 3_1^-$	41	2.336
3^-	3	3.063			2.694
3^-	4	3.151			2.701
3^-	5	3.276			
4^+	1	1.360	$2_1^+ \otimes 2_1^+$	88	1.249
4^+	2	2.191			1.958
4^+	3	2.335			
4^+	4	2.367			
4^+	5	2.524			
5^-	1	2.300			
6^+		2.139	$2_1^+ \otimes 2_1^+ \otimes 2_1^+$	88	1.747
6^+	2	2.291			
7^-	1	2.289			
8^+	1	2.345			
8^+	2	3.083			

[a] Taken from Ref. 65.

to the structure of the lowest $[2_1^+]_{\rm RPA}$ state displays similar characteristics to the ones discussed in Section 4 and shown in Table 6 for ^{144}Nd. Considering the relative sign of the main neutron and proton components, the $[2_1^+]_{\rm RPA}$ state is isoscalar and the $[2_2^+]_{\rm RPA}$ state is isovector. As discussed earlier (see Section 4 and eq. (12)), the quantity B is small for isoscalar states and large for isovector states. In our case, the magnitude of the quantity B and the structure of the $[2_2^+]_{\rm RPA}$ state support the interpretation of the third calculated 2^+ level as an isovector state.

Table 21. Quadrupole moment of the 2_1^+ state, strengths, mixing ratios and branching ratios of transitions in ^{124}Te calculated with the QPM in comparison with experimental data

Quantity	Theory	Experiment
$B(E1;0_1^+ \to 1_2^-)$[W.u.]	$5.6{\cdot}10^{-4}$	$4.7(4){\cdot}10^{-4(a)}$
$B(E1;0_1^+ \to 1_2^-)$[W.u.]	$4.5{\cdot}10^{-4}$	$6.5(9){\cdot}10^{-4(a)}$
$B(E2;2_3^- \to 1_1^-)[e^2fm^4]$	288	-
$B(E2;2_1^+ \to 0_1^+)[e^2fm^4]$	922	$1136(10)^{(b)}$
$B(E2;2_2^+ \to 0_1^+)[e^2fm^4]$	78	$38(1)^{(b)}$
$B(E2;4_1^+ \to 2_1^+)[e^2fm^4]$	290	$200^{(b)}$
$\delta(E2/M1;2_2^+ \to 2_1^+)$	-2.1	$-3.3(1)^{(b)}$
$\delta(E2/M1;2_3^+ \to 2_1^+)$	0.07	$0.13(12)^{(c)}$
$\delta(E2/M1;2_4^+ \to 2_1^+)$	0.26	$1.5(8)^{(b)}$
$B(E1;1_1^- \to 2_1^+)/B(E1;1_1^- \to 0_1^+)$	0.61	$0.18(5)^{(a)}$
$B(E1;1_2^- \to 2_1^+)/B(E1;1_2^- \to 0_1^+)$	0.01	$0.31(22)^{(a)}$
$B(E2;2_2^+ \to 2_1^+)/B(E2;2_2^+ \to$ g.s.)	31.2	$55.6(1)^{(c)}$
$B(E2;2_4^+ \to 2_2^+)/B(E2;2_4^+ \to 4_1^+)$	0.85	$1.00(33)^{(c)}$
$B(E2;4_2^+ \to 2_1^+)/B(E2;4_2^+ \to 4_1^+)$	0.02	$0.0062(16)^{(c)}$
$B(E2;2_4^+ \to 2_1^+)/B(E2;2_4^+ \to 4_1^+)$	0.04	$0.09(6)^{(c)}$
$B(E2;4_2^+ \to 2_2^+)/B(E2;4_2^+ \to 2_1^+)$	90.16	$4.8(3)^{(b)}$
$B(E2;4_2^+ \to 2_2^+)/B(E2;4_2^+ \to 4_1^+)$	1.42	$0.14(1)^{(b)}$
$B(E2;3_1^+ \to 2_2^+)/B(E2;3_1^+ \to 4_1^+)$	2.55	$5.3(3)^{(b)}$
$B(E2;3_1^+ \to 2_2^+)/B(E2;3_1^+ \to 2_1^+)$	33.52	$61(4)^{(b)}$
$Q_2(2_1^+)$	-40 efm^2	-45(4) $efm^{2(b)}$

[a] Taken from Ref. 65.
[b] Taken from Ref. 71.
[c] Taken from Ref. 70.

Another interesting phenomenon, observed in this nuclei, is the unusual γ-decay cascade after thermal neutron capture in ^{123}Te [65]. The analysis of the

experimental data [65, 73, 75], gives a clear evidence for a cascade, where the 3.101 MeV level decays via a very strong 353 keV transitions to the 1^- level at 2.747 MeV which itself populates the first excited state and the ground state. Whereas the decay of the 3.101 MeV level to the ground state is clearly suppressed because it requires a $M2$ transition, the surprising absence of other spin-allowed transitions to low-lying states has to be explained by the nuclear structure of the intermediate state.

A solution is suggested by the (γ, γ') results [65]. Here a ground-state $E1$ transition to the 2.747 MeV level with $B(E1) \uparrow = 0.47 \times 10^{-3}$ W.u. is observed which is unusually large for this mass region [57]. However, enhanced $E1$ transitions have recently been observed in the neighbouring ^{116,124}Sn isotopes as well [76]. It seems to be a typical phenomenon in nuclei near closed shells. The fast $E1$ transitions, as we have seen in Section 6, are considered to be a signature for quadrupole-octupole coupled states. For such a coupling a quintet of negative parity levels from 1^- to 5^- is predicted near to the sum energy of the 2_1^+ and 3_1^- phonon states [58]. The level in ^{124}Te lies at 2.747 MeV. This is nearly the sum energy of the first 2^+ state at 0.603 MeV and the first 3^- level at 2.294 MeV.

The two-phonon nature of the 1^- state at 2.747 MeV is strongly supported by the QPM results which can reproduce the transition strength and the branching ratios to the ground state and to the first 2^+ level. A sizeable direct two-phonon decay is possible within the QPM because of the RPA correlated ground state (see eq. (9)). In fact, one finds in general too large $B(E1)$ values, although, as discussed at length in Section 6, the mixing with the GDR is taken into account to a large extent in QPM. For the intermediate $\gamma-$cascade level at 3.101 MeV a dominant three-phonon structure is suggested. Such a 2^- state is predicted by the calculations at 3.770 MeV. In such a picture the experimentally observed decoupling from the low-lying dominant one-phonon states is naturally explained.

In a way similar to the decay of the 1_1^- level at 2.747 MeV, the second fast $E1$ transition in the (γ, γ') data from the 3.91 MeV state can be interpreted as the ground state decay of a multiphonon coupled state. Within the QPM the state would constitute the 1^- member of the $2_1^+ \otimes 2_1^+ \otimes 3_1^-$ multiplet. Again, the experimental strength of $B(E1) \uparrow = 6.5(9) \times 10^{-4}$W.u. can be well reproduced by such an assumption (see Table 20). However, sizeable decays to the 2_1^+ and 2_2^+ states not predicted by the QPM and the relatively large difference of about 600 keV compared to the $2_2^+ + 3_1^-$ sum energy point towards a more complex structure of this level. A possible explanation of both problems might be a significant anharmonicity as already suggested in Ref. 71 for the interpretation of the low-energy spectrum. However, the presence of a large three-phonon component is likely considering the successful explanation of the ground state coupling.

These results demonstrate that a microscopically based vibrational model is quite successful to explain many aspects of the structure of ^{124}Te. For the lowest

2^+ and 4^+ states this is not surprising in view of their pure phonon structure which was shown [77] to be a general phenomenon in virtually all even-even nuclei with $Z \geq 30$. However, the prevalence of multiphonon structures built on the octupole vibrations seems crucial for the explanation of the observed data.

On the other hand, open questions remain. As mentioned before neither the lowest 0^+ states nor the 6^+ states can be fully interpreted. Clearly, further experimental studies to establish complete experimental information, not only on the level scheme, but also on spectroscopic properties are required for a full understanding of the ^{124}Te structure. Additionally, the study of the evolution of prominent features like multiphonon structures in the chain of even-even tellurium isotopes will provide important insight.

8. CONCLUSION

There exists a wide-spread conviction that the low-lying excited states in atomic nuclei are well studied. Of course, this is true as far as our knowledge about the large components in the structure of the wave function is concerned. It is seen from this work that recent experimental results reveal very interesting properties of the excited states connected with the medium and even the small components in the structure of the wave function. The resulting picture turns out to be a very complicated one. The latter requires a substantial refinement of the theoretical models in order to get a deeper insight and understanding of the experimental data. Far from being sufficient, the contemporary nuclear models, including the QPM, allow for the investigation of these more complex phenomena. In particular, the delicate interaction between isovector and isoscalar degrees of freedom and between collective and noncollective modes, as well as the fast $E1$ transitions and other footprints of multiphonon states in even-even spherical nuclei, find a reasonably fair description within QPM in terms of the interaction between quasiparticles and phonons.

Acknowledgements

We acknowledge the useful discussions we have had with Prof. W. Andrejtscheff, Prof. I. Hamamoto, Prof. M. Kneissl, Dr. P. von Neumann-Cosel, Dr. V. Yu. Ponomarev, Dr. O. Scholten, Prof. V. G. Soloviev, Dr. A. I. Vdovin and Dr. V. V. Voronov. This work was partly supported by the Bulgarian Ministry of Science and Education under contract no. 626.

APPENDIX: QPM BACKGROUND

Following Refs. 2,3,17,18, we shall introduce some basic notations. The most general form of the model Hamiltonian is:

$$H = H_{sp} + H_{pair} + H_M^{ph} + H_{SM}^{ph} + H_M^{pp}, \tag{16}$$

where the term H_{sp} describes the motion of the independent nucleons in a self-consistent mean field; H_{pair} represents the monopole pairing interaction in the particle-particle channel; H_M^{ph} is a sum of isoscalar and isovector separable multipole interactions in the particle-hole channel; H_{SM}^{ph} is the same for the spin-multiple interaction and H_M^{pp} is the sum of the multipole interaction in the particle-particle channel (multipole pairing).

In the second quantized representation these terms can be written as:

$$H_{sp} = H_{sp}^n + H_{sp}^p = \sum_{jm} {}^n E_j a_{jm}^+ a_{jm} + \sum_{jm} {}^p E_j a_{jm}^+ a_{jm}, \tag{17}$$

$$H_M^{ph} = -\frac{1}{2} \sum_{\lambda\mu} \sum_{\tau,\rho=\pm 1} (\kappa_0^{(\lambda)} + \rho \kappa_1^{(\lambda)}) M_{\lambda\mu}^+(\tau) M_{\lambda\mu}(\rho\tau), \tag{18}$$

$$M_{\lambda\mu}^+(\tau) = \sum_{\substack{jj' \\ mm'}} \left\langle jm \left| i^\lambda R_\lambda(r) Y_{\lambda\mu}(\Omega) \right| j'm' \right\rangle a_{jm}^+ a_{j'm'}, \tag{19}$$

$$H_{SM}^{ph} = -\frac{1}{2} \sum_{LM} \sum_{\lambda=L,L\pm 1} \sum_{\tau,\rho=\pm 1} (\kappa_0^{(\lambda L)} + \rho \kappa_1^{(\lambda L)}) \left[S_{LM}^\lambda(\tau) \right]^+ \left[S_{LM}^\lambda(\rho\tau) \right], \tag{20}$$

$$\left[S_{LM}^\lambda(\tau) \right]^+ = \sum_{\substack{jj' \\ mm'}} \left\langle jm \left| i^\lambda R_\lambda(r) [\boldsymbol{\sigma}.\mathbf{Y}_{\boldsymbol{\lambda}}(\boldsymbol{\Omega})]_{LM} \right| j'm' \right\rangle a_{jm}^+ a_{j'm'}$$

$$[\boldsymbol{\sigma}.\mathbf{Y}_{\boldsymbol{\lambda}}(\boldsymbol{\Omega})]_{LM} = \sum_{\upsilon\mu} \langle 1\upsilon\lambda\mu \mid LM \rangle \, \sigma_\nu Y_{\lambda\mu},$$

$$\begin{aligned} H_M^{pp} = & -\frac{1}{2} \sum_{\lambda\mu} [G_n^{(\lambda)} P_{\lambda\mu}^+(n) P_{\lambda\mu}(n) + G_p^{(\lambda)} P_{\lambda\mu}^+(p) P_{\lambda\mu}(p) \\ & + G_{n,p}^{(\lambda)} (P_{\lambda\mu}^+(n) P_{\lambda\mu}(p) + P_{\lambda\mu}^+(p) P_{\lambda\mu}(n))], \end{aligned} \tag{21}$$

$$P_{\lambda\mu}^+(n) = \sum_{\substack{jj' \\ mm'}} {}^n \left\langle jm \left| i^\lambda R_\lambda(r) Y_{\lambda\mu}(\Omega) \right| j'm' \right\rangle (-)^{j'-m'} a_{jm}^+ a_{j'-m'}, \tag{22}$$

where $\widehat{j} = \sqrt{2j+1}$ and the operators a^+_{jm} and a_{jm} are respectively the creation and annihilation operators of nucleons with $j = \{nlj\}$; m, the magnetic quantum number; E_j, the energy of the corresponding single-particle state. The index τ is an isotopic index and takes two values $\tau = n, p$. Changing the sign of τ means changing the type of particles: $n \to p$ and $p \to n$. The quantities G_n and G_p are the neutron-neutron and proton-proton pairing interaction constants. The constants of the isoscalar and isovector terms of the multipole-multipole (spin-multipole) interaction are denoted by $\kappa_0^{(\lambda)}(\kappa_0^{(\lambda L)})$ and $\kappa_1^{(\lambda)}(\kappa_1^{(\lambda L)})$, respectively. These constants are related to the neutron-neutron $\kappa_{nn}^{(\lambda)}$, proton-proton $\kappa_{pp}^{(\lambda)}$ and neutron-proton $\kappa_{pp}^{(\lambda)}$ multipole and spin-multipole interaction constants in the following manner:

$$\begin{aligned} \kappa_{nn}^{(\lambda)} &= \kappa_{pp}^{(\lambda)} = \kappa_0^{(\lambda)} + \kappa_1^{(\lambda)}, \\ \kappa_{np}^{(\lambda)} &= \kappa_0^{(\lambda)} - \kappa_1^{(\lambda)}. \end{aligned}$$

The quantities $G_n^{(\lambda)}, G_p^{(\lambda)}$ and $G_{np}^{(\lambda)}$ are the constants of the multipole pairing. In the present implementation of the model, the particle-particle channel can be switched on in addition to the multipole-multipole interaction in the cases where it is estimated to be important (usually for the quadrupole-quadrupole and octupole-octupole channels). It should be noted here that the monopole pairing interaction is also realized by using this channel and not the formulas that can be derived specifically for the pairing case [3]. The radial dependence of the interaction $R_\lambda(r)$ can be either $R_\lambda(r) \sim r^\lambda$ or $R_\lambda(r) \sim dV(r)/dr$, where $V(r)$ is the central part of the single-particle potential.

The Bogoliubov canonical transformation from nucleon creation and annihilation operators a^+_{jm} and a_{jm} to quasiparticle creation and annihilation operators α^+_{jm} and α_{jm} is taken in the standard form:

$$a_{jm} = u_j \alpha_{jm} + (-)^{j-m} v_j \alpha^+_{j-m}. \tag{23}$$

Using the transformation (23), we can re-express the model Hamiltonian in terms of quasiparticles. For example, the term H_{sp} takes the form :

$$H_{sp} = \sum_{jm}{}^n \varepsilon_j \alpha^+_{jm} \alpha_{jm} + \sum_{jm}{}^p \varepsilon_j \alpha^+_{jm} \alpha_{jm}, \tag{24}$$

where the quasiparticle energy is given by:

$$\varepsilon_j = [(E_j - \lambda_\tau)^2 + C_\tau^2]^{1/2}.$$

The chemical potential λ_τ and correlation function (energy gap) C_τ are calculated according to the well-known BCS equations [2]. The particle-hole operator $M^+_{\lambda\mu}(\tau)$ (eq. (19)) can be written in the form:

$$M^+_{\lambda\mu}(\tau) = \frac{1}{\hat{\lambda}} \sum_{jj'}{}^{\tau} f^{(\lambda)}_{jj'} \{ \frac{1}{2} u^{(+)}_{jj'} [A^+(jj'\lambda\mu) +$$

$$+(-1)^{\lambda-\mu} A(jj'\lambda-\mu)] + v^{(-)}_{jj'} B(jj'\lambda\mu)\}, \tag{25}$$

and the particle-particle operator $P^+_{\lambda\mu}(\tau)$ (eq. (22)) becomes:

$$P^+_{\lambda\mu}(\tau) = \frac{1}{\hat{\lambda}} \sum_{jj'}{}^{\tau} f^{(\lambda)}_{j_1 j_2} [u_j u_{j'} A^+(jj'\lambda\mu) -$$

$$-(-1)^{\lambda-\mu} v_j v_{j'} A(jj'\lambda-\mu) - 2u_j v_{j'} B(jj'\lambda\mu)], \tag{26}$$

where

$$A^+(jj'\lambda\mu) = \sum_{mm'} < jmj'm' \mid \lambda\mu > \alpha^+_{jm} \alpha^+_{j'm'}, \tag{27}$$

$$A(jj'\lambda\mu) = \left[A^+(jj'\lambda\mu)\right]^+ \tag{28}$$

$$B^+(jj'\lambda\mu) = \sum_{mm'} (-1)^{j'+m'} < jmj'm' \mid \lambda\mu > \alpha^+_{jm} \alpha_{j'-m'}, \tag{29}$$

and the quantities $f^{(\lambda)}_{jj'}$ are the reduced single-particle matrix elements of the operator $i^\lambda R_\lambda(r) Y_{\lambda\mu}(\Omega)$.

The RPA phonon creation operator is taken as a superposition of the operators (27) and (28):

$$Q^+_{\lambda\mu i} = \frac{1}{2} \sum_{\tau}{}^{n,p} \sum_{jj'} \{ \psi^{\lambda i}_{jj'} A^+(jj'\lambda\mu) - (-1)^{\lambda-\mu} \varphi^{\lambda i}_{jj'} A(jj'\lambda-\mu)\}, \tag{30}$$

where $\psi^{\lambda i}_{jj'}$ and $\varphi^{\lambda i}_{jj'}$ are the forward and backward RPA amplitudes, respectively. The energy of the phonons $\omega_{\lambda i}$ and the amplitudes $\psi^{\lambda i}_{jj'}$ and $\varphi^{\lambda i}_{jj'}$ are obtained by solving the RPA equations. The general form of the equations in the case of separable interaction is given in Refs. 2,3.

The operator $P^+_{\lambda\mu}(\tau)$ (see eqs. (22) and (26)), can be rewritten in terms of the phonon operators (30) and the operators (29) as follows:

$$\begin{aligned} P^+_{\lambda\mu}(\tau) \quad = \quad & \hat{\lambda} \{ \frac{1}{2} \sum_i [(L^{(\lambda i)} + M^{(\lambda i)}) Q^+_{\lambda\mu i} - \\ & -(L^{(\lambda i)} - M^{(\lambda i)})(-1)^{\lambda-\mu} Q_{\lambda-\mu i} - \\ & -2(-1)^{\lambda-\mu} \sum_{j_1 j_2} \Theta^{(\lambda)}_{j_1 j_2} B^+(j_1 j_2 \lambda-\mu)\}, \end{aligned} \tag{31}$$

where

$$L^{(\lambda i)} = \sum_{\tau} L_{\tau}^{(\lambda i)} = \sum_{\tau} \sum_{j_1 j_2}{}^{\tau} f_{j_1 j_2}^{(\lambda)} v_{j_1 j_2}^{(-)} g_{j_1 j_2}^{(\lambda i)}, \tag{32}$$

$$M^{(\lambda i)} = \sum_{\tau} M_{\tau}^{(\lambda i)} = \sum_{\tau} \sum_{j_1 j_2}{}^{\tau} f_{j_1 j_2}^{(\lambda)} v_{j_1 j_2}^{(+)} w_{j_1 j_2}^{(\lambda i)}, \tag{33}$$

$$\Theta_{j_1 j_2}^{(\lambda)} = f_{j_1 j_2}^{(\lambda)} u_{j_2} v_{j_1} \tag{34}$$

and

$$\begin{aligned} g_{j_1 j_2}^{(\lambda i)} &= \psi_{j_1 j_2}^{\lambda i} + \varphi_{j_1 j_2}^{\lambda i}, \\ w_{j_1 j_2}^{(\lambda i)} &= \psi_{j_1 j_2}^{\lambda i} - \varphi_{j_1 j_2}^{\lambda i}. \end{aligned} \tag{35}$$

A similar form could be found for the operators $M_{\lambda\mu}^{+}(\tau)$ and $S_{LM}^{+}(\tau)$ [2,18]. For the multipole-multipole operators one gets:

$$M_{\lambda\mu}^{+}(\tau) = \frac{1}{\hat{\lambda}} \{ \frac{1}{2} \sum_{i} R^{(\lambda i)} (Q_{\lambda\mu i}^{+} + (-1)^{\lambda-\mu} Q_{\lambda-\mu i}) + \sum_{j_1 j_2} \xi_{j_1 j_2}^{(\lambda)} B(j_1 j_2 \lambda\mu) \}, \tag{36}$$

where

$$R^{(\lambda i)} = \sum_{\tau} R_{\tau}^{(\lambda i)} = \sum_{j_1 j_2}{}^{\tau} f_{j_1 j_2}^{(\lambda)} v_{j_1 j_2}^{(-)} \tag{37}$$

and

$$\xi_{j_1 j_2}^{(\lambda)} = f_{j_1 j_2}^{(\lambda)} v_{j_1 j_2}^{(-)}. \tag{38}$$

Taking into account the above equations, the terms in the general model Hamiltonian (16) responsible for the interaction of quasiparticles and phonons, acquire the following form:

$$\begin{aligned} H_{qp-ph} &= \sum_{\lambda\mu i} (-1)^{\lambda-\mu} \frac{1}{\sqrt{2\mathcal{Y}_{\lambda i}}} \sum_{\tau} \{ [(\mathfrak{L}_{\tau}^{(\lambda i)} + \mathfrak{M}_{\tau}^{(\lambda i)}) Q_{\lambda\mu i}^{+} + \\ &+ (-1)^{\lambda-\mu} (\mathfrak{L}_{\tau}^{(\lambda i)} - \mathfrak{M}_{\tau}^{(\lambda i)}) Q_{\lambda-\mu i}] \sum_{j_1 j_2}{}^{\tau} \Theta_{j_1 j_2}^{(\lambda)} B(j_1 j_2 \lambda - \mu) - \\ &- \frac{1}{2} \mathfrak{R}_{\tau}^{(\lambda i)} (Q_{\lambda\mu i}^{+} + (-1)^{\lambda-\mu} Q_{\lambda-\mu i}) \sum_{j_1 j_2}{}^{\tau} \xi_{j_1 j_2}^{(\lambda)} B(j_1 j_2 \lambda - \mu) + h.c. \}, \end{aligned} \tag{39}$$

where

$$\sqrt{\frac{2}{\mathcal{Y}_{\lambda i}}}\mathfrak{L}_{\tau}^{(\lambda i)} = G_{n}^{(\lambda)}L_{\tau}^{(\lambda i)} + G_{np}^{(\lambda)}L_{-\tau}^{(\lambda i)},$$

$$\sqrt{\frac{2}{\mathcal{Y}_{\lambda i}}}\mathfrak{M}_{\tau}^{(\lambda i)} = G_{n}^{(\lambda)}M_{\tau}^{(\lambda i)} + G_{np}^{(\lambda)}M_{-\tau}^{(\lambda i)}, \tag{40}$$

$$\sqrt{\frac{2}{\mathcal{Y}_{\lambda i}}}\mathfrak{R}_{\tau}^{(\lambda i)} = (\kappa_{0}^{(\lambda)} + \kappa_{1}^{(\lambda)})R_{\tau}^{(\lambda i)} + (\kappa_{0}^{(\lambda)} - \kappa_{1}^{(\lambda)})R_{-\tau}^{(\lambda i)}.$$

The quantities $\mathcal{Y}_{\lambda i}$ [3] are calculated at the RPA level, using the normalization condition for the forward and backward amplitudes:

$$\frac{1}{2}\sum_{j_1 j_2}[(\psi_{jj'}^{\lambda i})^2 - (\varphi_{jj'}^{\lambda i})^2] = 1. \tag{41}$$

Introducing the notation:

$$\mathcal{K}_{\tau}^{(\pm)}(j_1 j_2 \lambda i) = \frac{f_{j_1 j_2}^{(\lambda)}}{\sqrt{\mathcal{Y}_{\lambda i}}}[v_{j_1 j_2}^{(-)}\mathfrak{R}_{\tau}^{(\lambda i)} - (u_{j_2 j_1}^{(+)} + u_{j_2 j_1}^{(-)})(\mathfrak{L}_{\tau}^{(\lambda i)} \pm \mathfrak{M}_{\tau}^{(\lambda i)})], \tag{42}$$

eq. (39) finally takes the form:

$$\begin{aligned} H_{qp-ph} \quad = \quad & -\frac{1}{2\sqrt{2}}\sum_{\lambda\mu i}\{(-1)^{\lambda-\mu}\sum_{\tau}\sum_{j_1 j_2}[\mathcal{K}_{\tau}^{(+)}(j_1 j_2 \lambda i)Q_{\lambda\mu i}^{+} \\ & +(-1)^{\lambda-\mu}\mathcal{K}_{\tau}^{(-)}(j_1 j_2 \lambda i)Q_{\lambda-\mu i}]B(j_1 j_2 \lambda-\mu) + h.c.\}. \end{aligned} \tag{43}$$

The influence of the particle-particle channel is switched off if the terms $\mathfrak{L}_{\tau}^{(\lambda i)}$ and $\mathfrak{M}_{\tau}^{(\lambda i)}$ are equal to zero. In that case, the interaction between quasiparticles and phonons of eq. (43) takes the well-known form for the particle-hole channel taken alone [3, 18].

The matrix element H_{qp-ph} (see eq. (43)), between a one- and a two-phonon state has the form:

$$S_{\lambda_2 i_2}^{\lambda_1 i_1}(Ji) \equiv \left\langle Q_{JMi}\left|H_{qp-ph}\right|Q_{\lambda_1\mu_1 i_1}^{+}Q_{\lambda_2\mu_2 i_2}^{+}\right\rangle = \tag{44}$$

$$-\frac{1}{\sqrt{2}}\hat{\lambda}_1\hat{\lambda}_2\sum{}^{\tau}\sum_{j_1 j_2 j_3}{}^{\tau}\{(-1)^{j_1+j_2+J}\left\{\begin{array}{ccc} J & \lambda_1 & \lambda_2 \\ j_3 & j_2 & j_1 \end{array}\right\}$$

$$\times[\varphi^{\lambda_1 i_1}_{j_1 j_3}\psi^{\lambda_2 i_2}_{j_3 j_2}\mathcal{K}^{(+)}_{\tau}(j_1 j_2 J i)+\psi^{\lambda_1 i_1}_{j_1 j_3}\varphi^{\lambda_2 i_2}_{j_3 j_2}\mathcal{K}^{(-)}_{\tau}(j_1 j_2 J i)]$$
$$+(-1)^{j_1+j_2+\lambda_1}\left\{\begin{array}{ccc}\lambda_1 & J & \lambda_2\\ j_3 & j_2 & j_1\end{array}\right\}$$
$$\times[\psi^{Ji}_{j_1 j_3}\psi^{\lambda_2 i_2}_{j_3 j_2}\mathcal{K}^{(-)}_{\tau}(j_1 j_2 \lambda_1 i_1)+\varphi^{Jk}_{j_1 j_3}\varphi^{\lambda_2 i_2}_{j_3 j_2}\mathcal{K}^{(+)}_{\tau}(j_1 j_2 \lambda_1 i_1)]$$
$$+(-1)^{j_1+j_2+\lambda_2}\left\{\begin{array}{ccc}\lambda_2 & \lambda_1 & J\\ j_3 & j_2 & j_1\end{array}\right\}$$
$$\times[\varphi^{\lambda_1 i_1}_{j_1 j_3}\varphi^{Ji}_{j_3 j_2}\mathcal{K}^{(-)}_{\tau}(j_1 j_2 \lambda_2 i_2)+\psi^{\lambda_1 i_1}_{j_1 j_3}\psi^{Jk}_{j_3 j_2}\mathcal{K}^{(+)}_{\tau}(j_1 j_2 \lambda_2 i_2)]\},$$

where the quantities in curly brackets are the $6j$ symbols [20].

If $\mathfrak{L}^{(\lambda_i)}_{\tau}=0$ and $\mathfrak{M}^{(\lambda_i)}_{\tau}=0$ (i.e., the particle-particle channel is turned off), the quantity $\mathcal{K}^{(\pm)}_{\tau}$ reduces to the following expression:

$$\mathcal{K}^{(+)}_{\tau}(j_1 j_2 \lambda i)=\mathcal{K}^{(-)}_{\tau}(j_1 j_2 \lambda i)=f^{(\lambda)}_{j_1 j_2}v^{(-)}_{j_1 j_2}\mathcal{Y}^{-\frac{1}{2}}_{\lambda i}$$

and $S^{\lambda_1 i_1}_{\lambda_2 i_2}(Ji)$ becomes [3]:

$$\begin{aligned}S^{\lambda_1 i_1}_{\lambda_2 i_2}(Ji) \;=\; & U^{\lambda_1 i_1}_{\lambda_2 i_2}(Ji)= \\ & (-)^{\lambda_1+\lambda_2-\lambda}\frac{1}{\sqrt{2}}(2\lambda_1+1)^{1/2}(2\lambda_2+1)^{1/2}\sum_{\tau}\sum_{j_1 j_2 j_3}{}^{\tau}\, v^{(\mp)}\times \\ & \frac{f^{\lambda_2}_{j_1 j_2}}{\sqrt{y^{\lambda_2 i_2}}}\left\{\begin{array}{ccc}\lambda_1 & \lambda_2 & \lambda\\ j_1 & j_3 & j_2\end{array}\right\}\left(\psi^{\lambda i}_{j_3 j_1}\psi^{\lambda_1 i_1}_{j_2 j_3}+\phi^{\lambda i}_{j_3 j_1}\phi^{\lambda_1 i_1}_{j_2 j_3}\right)+ \\ & \frac{f^{\lambda_1}_{j_1 j_2}}{\sqrt{y^{\lambda_1 i_1}}}\left\{\begin{array}{ccc}\lambda_1 & \lambda_2 & \lambda\\ j_3 & j_2 & j_1\end{array}\right\}\left(\phi^{\lambda i}_{j_2 j_3}\phi^{\lambda_2 i_2}_{j_3 j_1}+\psi^{\lambda i}_{j_2 j_3}\psi^{\lambda_2 i_2}_{j_3 j_1}\right)+ \\ & \frac{f^{\lambda}_{j_1 j_2}}{\sqrt{y^{\lambda i}}}\left\{\begin{array}{ccc}\lambda_1 & \lambda_2 & \lambda\\ j_2 & j_1 & j_3\end{array}\right\}\left(\psi^{\lambda_1 i_1}_{j_3 j_1}\phi^{\lambda_2 i_2}_{j_2 j_3}+\phi^{\lambda_1 i_1}_{j_3 j_1}\psi^{\lambda_2 i_2}_{j_2 j_3}\right), \qquad (45)\end{aligned}$$

which is the matrix coupling states differing by one phonon in the case when only the particle-hole channel is switched on.

REFERENCES

1. **Bohr A., Mottelson B.R.** — Nuclear Structure, New York, Benjamin, v.2, 1975.
2. **Soloviev V.G.** — Theory of Complex Nuclei, Oxford, Pergamon Press, 1976.
3. **Soloviev V.G.** — Theory of Atomic Nuclei: Quasiparticles and Phonons, Bristol, IOP, 1992.
4. **Silvestre-Brac B., Piepenbring R.** — Phys. Rev., 1982, v.C 26, p.2640;
   Piepenbring R., Protasov K.V., Silvestre-Brac B. — Nucl. Phys., 1995, v.A 586, p.396, p.413;
   Grinberg M., Piepenbring R., Protasov K.V., Silvestre-Brac B. — Nucl. Phys., 1995, v.A 597, p.355.

5. **Marumori T.** — Prog. Theor. Phys., 1960, v.24, p.331.
6. **Belyaev S.T., Zelevinsky V.G.** — Nucl. Phys., 1962, v.A39, p.582.
7. **Klein A., Marshalek E.R.** — Rev. Mod. Phys., 1991, v.63, p.375.
8. **Arima A., Iachello F.** — Ann. Phys. (N.Y.), 1976, v.99, p.253;
Arima A., Iachello F. — Phys. Rev., 1976, v.C 14, p.761.
9. **Soloviev V.G., Stoyanov Ch., Nikolaeva R.** — JINR Communication E-83-166, Dubna, 1983.
10. **Paar V., Vorkapič D., Dieperink A.E.L.** — Phys. Rev. Lett., 1992, v.69, p.2184;
Soloviev V.G. — Nucl. Phys., 1993, v.A 554, p.77.
11. **Grinberg M., Stoyanov Ch.** — Contributions to the International Conference "Selected Topics in Nuclear Structure", JINR, D4-89-326, Dubna, 1989, p.16.
12. **Grinberg M.** — Bulg. J. Phys, 1991, v.18, p.263.
13. **Adam J., Dobeš J., Kracík B. et al.** — Z. Phys., 1992, v.A 343, p.381.
14. **Thai Thac Dinh, Grinberg M., Stoyanov C.** — J. Phys., 1992, v.G 18, p.329.
15. **Grinberg M., Thai Thac Dinh, Protochristov Ch.** — J. Phys., 1993, v.G 19, p.1179.
16. **Grinberg M., Stoyanov Ch.** — Nucl. Phys., 1994, v.A 573, p.231.
17. **Vdovin A.I., Soloviev V.G.** — Sov. J. Part. Nucl. (Elementarnie Tchastitsi i Atomnie Jadra), 1983, v.14, p.237.
18. **Voronov V.V., Soloviev V.G.** — Sov. J. Part. Nucl. (Elementarnie Tchastitsi i Atomnie Jadra), 1983, v.14, p.1380.
19. **Gales S., Stoyanov C., Vdovin A.I.** — Phys. Rep., 1988, v.166, p.125.
20. **Varshalovich D.A., Moskalev A.N., Khersonskii V.K.** — Quantum Theory of Angular Momentum, Singapore, World Scientific, 1988.
21. **Bertsch G.F., Bortignon P.F., Broglia R.A.** — Rev. Mod. Phys., 1983, v.55, p.287.
22. **Vdovin A.I., Stoyanov Ch.** — Izv. AN SSSR, Ser. fiz., 1973, v.37, p.1750.
23. **Mitroshin V.E.** — Izv. AN SSSR, Ser. fiz., 1974, v.38, p.811.
24. **Chepurnov V.A.** — Sov. J. Nucl. Phys, 1967, v.6, p.955.
25. **Takeuchi K., Moldauer P.A.** — Phys. Lett., 1969, v.B 28, p.384.
26. **Cottle P.D., Aziz S.M., Kemper K.W. et al.** — Phys. Rev., 1991, v.C 43, p.59.
27. **Enghard W., Käubler L., Prade H. et al.** — Nucl.Phys., 1986, v.A 449, p.417.
28. **Sandor R.K. J., Block H.P., Garg U. et al.** — Nucl. Phys., 1991, v.A 535, p.669.
29. **Spear R.H.** — Atomic Data and Nuclear Data Tables, 1989, v.42, p.55.
30. **Raman S., Malarkey C.H., Milner W.I. et al.** — Atomic Data and Nuclear Data Tables, 1989, v.42, p.1.
31. **Meyer R.A., Scholten O., Brant S., Paar V.** — Phys. Rev., 1990, v.C 41, p.2386.
32. **Raman S., Auble R.I., Ball J.B. et al.** — Phys. Rev., 1976, v.C 14, p.1381.
33. **Copnell J., Robinson S., Heyde K. et al.** — Phys. Lett., 1989, v.B 222, p.1.
34. **Hamilton W.D., Irbäck A., Elliott J.P.** — Phys. Rev. Lett., 1984, v.26, p.2469.
35. **Van Isacker P., Heyde K., Jolie J. et al.** — Ann. Phys., 1986, v.171, p.253.
36. **Nojarov R., Faessler A. J.** — J. Phys., 1987, v.G 13, p.337.
37. **Elliot J.P.** — Rep. Prog. Phys., 1985, v.48, p.171.

38. **Gupta J.B.** — Nucl. Phys., 1988, v.A 484, p.189.

39. **Lipas P.O.** — Rep. Prog. Phys., 1990, v.53, p.1355.

40. **Robinson S.J., Jolie J., Copnell J.** — Private communication and Proceedings of the 7th International Symposium on Capture Gamma-Ray Spectroscopy and Related Topics, Asilomar, California, 1990.

41. **Nikolaeva R., Stoyanov C., Vdovin A.I.** — Europhys. Lett., 1989, v.8, p.117.

42. **Scholten O., Heyde K., Van Isacker P. et al.** — Nucl. Phys., 1985, v.A 438, p.41.

43. **Richter A.** — Nucl. Phys., 1991, v.A 522, p.139c.

44. **Demidov A.M., Govor L.I., Kurkin V.A., Mihajlov I.V.** — Yad. Phys., 1997, v.60, p.581.

45. **Arima A., Otsuka T., Iachello F., Talmi I.** — Phys. Lett., 1977, v.B 66, p.205;
Otsuka T., Arima A., Iachello F., Talmi I. — Phys. Lett., 1978, v.B 76, p.139.

46. **Kraciková T.I., Finger M., Pavlov V.N. et al.** — J. Phys, 1984, v.G 10, p.571.

47. **Scholten O., Iachello F., Arima A.** — Ann. Phys. (N.Y.), 1978, v.115, p.325.

48. **Barfield A.F., von Brentano P., Dewald A. et al.** — Z. Phys., 1989, v.A 332, p.29.

49. **Pitz H.H., Heil R.D., Kneissl U. et al.** — Nucl. Phys., 1990, v.A 509, p.587.

50. **Gatenby R.A., Vanhoy J.R., Baum E.M. et al.** — Phys. Rev., 1990, v.C 41, p.R414.

51. **Gatenby R.A., Johnson E.L., Baum E.M. et al.** — Nucl. Phys., 1993, v.A 560, p.633.

52. **Kneissl M., Pitz H.H., Zilges H.** — Prog. Part. Nucl. Phys., 1996, v.37, p.349.

53. **Herzberg R.-D., Bauske I., von Bretano P. et al.** — Nucl. Phys, 1995, v.A 592, p.211.

54. **Wilhelm M., Radermacher E., Zilges A., von Brentano P.** — Phys. Rev., 1996, v.C 54, p.449.

55. **Eckert T., Beck O., Besserer et al.** — Phys. Rev., 1997, v.C 56, p.1256.

56. **Andrejtscheff W., Schilling K.D., Manfrass P.** — Atomic Data and Nuclear Data Tables, 1975, v.16, p.515.

57. **Endt P.M.** — Atomic Data and Nuclear Data Tables, 1987, v.26, p.47.

58. **Vogel P., Kocbach L.** — Nucl. Phys., 1971, v.A 176, p.33.

59. **Voronov V.V., Dao Tien Khoa** — JINR Preprint, P4-83-174, Dubna, 1983;
Voronov V.V., Dao Tien Khoa, Ponomarev V.Yu. — Izv. AN SSSR, Ser. fiz., 1984, v.48, p.1846.

60. **Soloviev V.G., Sushkov A.V.,** — Phys. Lett., 1991, v.B 262, p.189.

61. **Kusnezov D.F., Henry E.A., Meyer R.A.** — Phys. Lett., 1989, v.B 228, p.11.

62. **Losano L., Dias H., Krmpotic F., Wildenthal B.H.** — Phys. Rev., 1988, v.C 38, p.2902.

63. **Müller-Zanotti E., Hertenberger R., Kader H. et al.** — Phys. Rev., 1993, v.C 47, p.2524.

64. **Hamamoto I.** — Nucl. Phys., 1973, v.A 205, p.225;
Hamamoto I. — Nucl. Phys., 1993, v.A 557, p.515.

65. **Georgii R., von Neumann-Cosel P., von Egidy T. et al.** — Phys. Lett., 1995, v.B 351, p.82;
Georgii R., von Egidy T., Klora J. et al. — Nucl. Phys., 1995, v.A 592, p.307.

66. **Robinson S.J., Hamilton W.D., Snelling D.M. et al.** — J. Phys., 1983, v.G 9, p.961.

67. **Mardirosian G., Stewart N.M.** — Z. Phys., 1984, v.A 315, p.213.

68. **Jianming Y., Yunzuo L., Dailing H.** — Z. Phys., 1988, v.A 331, p.803.

69. **Rikovska J., Stone N.J., Walker P.M., Waltres W.B.** — Nucl. Phys, 1989, v.A 505, p.145.

70. **Lee C.S., Cizewski J.A., Barker D.** — Nucl. Phys., 1991, v.A 530, p.58.

71. **Casten R.F., Zhiang J.-Y., Liao B.-C.** — Phys. Rev., 1991, v.C 44, p.523.

72. **Goswamy J., Chand B., Mehta D., Singh N., Trehan P.N.** — Int. J. Appl. Radiat. Isot., 1993, v.44, p.541.

73. **Bushnell D.L., Chaturvedi R.P., Smither R.K.** — Phys. Rev., 1969, v.179, p.1113.

74. **Cizewski J.A.** — Phys. Lett., 1989, v.B 219, p.189.

75. **Mughabghab S.F., Divadeenam M., Holden N.E.** — Neutron Cross Section, New York, Academic Press, v.1, 1981.

76. **Govaert K., Govor E., Jacobs D. et al.** — Phys. Lett., 1994, v.B 335, p.113.

77. **Pietralla N., von Brentano P., Casten R.F., Otsuka T., Zamfir N.V.** — Phys. Rev. Lett., 1994, v.73, p.2962.

78. **Cizewski J.A., Bernstein L.A., Henry R.G. et al.** — Proc. 8th Int. Conf. on Capture Gamma-Ray Spectroscopy, ed. J. Kern, Singapore, World Scientific, 1994, p.328.

79. **Belgya T., Gatenby R.A., Baum E.M. et al.** — Phys. Rev., 1995, v.C 52, p.R2314.
Zilges A., von Brentano P., Herzberg R.-D. et al. — Nucl. Phys., 1996, v.A 599, p.147c.

80. **Robinson S.J., Jolie J., Börner H.G. et al.** — Phys. Rev. Lett., 1994, v.73, p.412.

81. **Perrino R., Blasi N., De Leo R. et al.** — Nucl. Phys., 1993, v.A 561, p.343.

82. **Vanhoy J.R., Anthony J.M., Haas B.M. et al.** — Phys. Rev., 1995, v.C 52, p.2387.

83. **Leder C.M., Shirley V.S.** — Tables of Isotopes, 7th edition, New York, Wiley, 1978.

84. **Ravinder K., Sharma K., Sooh S., Trehnan P.N.** — J. Phys. Soc. Jpn, 1980, v.49, p.2122.

85. **Peker L.K.,** — Nucl. Data Sheets, 1984, v.41, p.195; 1990, v.60, p.953.